Journal
Journal of Engineering Mechanics, 150(5)

ISSN
0733-9399

Authors
Montalto, Eduardo J
Konstantinidis, Dimitrios

Publication Date
2024-05-01

DOI
10.1061/jenmdt.emeng-7395

Effective Warping Properties and Buckling Analysis of Fiber-Reinforced Elastomeric Isolators

Eduardo J. Montalto[1] and Dimitrios Konstantinidis[2]

[1]Ph.D Candidate, Dept. of Civil and Environmental Engineering, Univ. of California, Berkeley, CA 94720. Email: eduardo_montalto@berkeley.edu

[2]Associate Professor, Dept. of Civil and Environmental Engineering, Univ. of California, Berkeley, CA 94720 (corresponding author). Email: konstantinidis@berkeley.edu

Abstract

Fiber-reinforced elastomeric isolators (FREIs) have been proposed as a cost-effective solution for expanding the use of seismic isolation to normal-importance structures. By using lightweight fiber reinforcement and eliminating the attachment plates, FREIs reduce cost while improving the isolation efficiency and reducing tensile stresses in the rubber. However, the flexural flexibility of the fiber allows cross-sectional distortions (i.e., warping) to occur, which significantly impacts the stability of these devices. This paper evaluates the buckling of rectangular, circular and annular FREIs, taking into account shear warping effects. A planar buckling theory previously proposed by the authors is adapted for the three-dimensional problem, and effective warping rigidities and warping-related areas are derived for the above bearing geometries, accounting for rubber compressibility. To assess the adequacy of the proposed buckling theory and derived warping properties in predicting the buckling of FREIs, a parametric finite element study is conducted. The critical load predictions of the proposed analytical formulation are found to be in excellent agreement with those of the numerical simulations. It is shown that traditional estimations of the buckling load that neglect warping are significantly unconservative. Finally, design recommendations and resources are provided for practice-oriented applications.

Keywords: Shear warping; Warping rigidity; Buckling theory; Fiber reinforced elastomeric isolators (FREIs); Stability of elastomeric bearings; Seismic isolation

INTRODUCTION

Elastomeric isolators consisting of thin rubber layers interleaved by reinforcement layers are vulnerable to buckling under compressive loads due to their high flexibility in shear. Haringx's buckling theory (1949), originally developed for helical springs and solid rubber rods, was adopted by Gent (1964) to study the buckling of thin rubber blocks bonded to steel plates, and has now become widely accepted to evaluate the stability of traditional steel-reinforced elastomeric isolators (SREIs) (Kelly and Konstantinidis 2011). Haringx's buckling load is given by:

$$P_{cr}^{H} = \frac{-P_S + \sqrt{P_S^2 + 4P_S P_E}}{2} \tag{1}$$

where $P_S = GA$ = the shear rigidity, $P_E = \pi^2 EI/h^2$ = Euler's critical load, and EI = the bending rigidity. In the context of SREIs, GA_b and $\widetilde{EI}_b$ should be used instead, where $GA_b = GA(h/t_r)$ = the shear rigidity of the multilayer bearing, $\widetilde{EI}_b = \widetilde{EI}(h/t_r)$ = the *effective* bending rigidity of the multilayer bearing, $\widetilde{EI}$ = the *effective* bending rigidity of a single rubber layer, h = total height of the bearing, and t_r = total height of rubber. Haringx's buckling load is derived from a one-dimensional beam theory which assumes that cross-sectional planes remain plane after deformation, but not orthogonal to the deformed axis, therefore allowing for shear deformations. This is suitable for SREIs where the steel plates are thick and very rigid in bending, and thus prevent cross-sectional distortions. However, this is not the case when the reinforcement is flexible in bending, as in the case of fiber-reinforced elastomeric isolators (FREIs), and cross-sectional warping due to transverse shear (i.e., shear warping) needs to be accounted for.

The first study concerning the buckling behavior of planar elastomeric bearings accounting for the impact of reinforcement flexural flexibility is by Simo (1982). Later, Kelly (1994) introduced an alternative formulation, which was later extended by Tsai and Kelly (2005a, 2005b). Both formulations, despite yielding significantly different results, predicted an important reduction in P_{cr}

with respect to Haringx's buckling load estimate. Recently, the stability of short beams accounting for shear warping has been revisited in (Montalto and Konstantinidis, "Buckling of short beams", submitted, *J. Eng. Mech.*, ASCE). A buckling formulation was derived from the consistent linearization of a fully geometrically nonlinear planar beam accounting for warping where the finite deformation field was posed as that of a constrained director Cosserat rod. The resulting theory generalizes the one by Kelly and Tsai, and accounts for warping effects as well as axial shortening of the element. Its applicability to FREIs was verified using a parametric finite element study of infinite strip isolators, where the predictions of the analytical formulation were shown to be in excellent agreement with results from the numerical simulations. This study also provided a comparison with respect to previous buckling formulations that account for warping.

The buckling formulation presented in (Montalto and Konstantinidis, "Buckling of short beams", submitted, *J. Eng. Mech.*, ASCE), as well as the earlier one by Kelly and Tsai, make use of an *effective* isolator warping rigidity and warping-related cross-sectional areas. These were derived for an infinite strip bearing by Tsai and Kelly (2005a) accounting for fiber extensibility, and extended in (Montalto and Konstantinidis, "Buckling of short beams", submitted, *J. Eng. Mech.*, ASCE) to also consider rubber compressibility. Both of these results are based on the usual kinematic assumptions of a parabolic bulging shape and linear variation of displacements through the thickness of the rubber layer, and the assumption that normal stresses in the rubber are dominated by the pressure, leading to the so-called *pressure solution*. The warping properties of an infinite strip bearing were also derived by Pinarbasi and Mengi (2008, 2017) using an approximate formulation based on a modified Galerkin method which uses weighted averages of displacements and stresses through the layer thickness, and does not depend on the assumptions cited before; reinforcement flexibility and rubber compressibility were considered. Despite recognition of the significant effect of warping on the mechanical response of FREIs since their inception (Kelly 1999), warping for bearing geometries other than infinite strip has been unexplored thus far (Van Engelen 2019).

The present study investigates the warping response of three-dimensional FREIs and the impact of warping on their stability under compressive loads. First, the buckling theory presented in (Montalto and Konstantinidis, "Buckling of short beams", submitted, *J. Eng. Mech.*, ASCE) is revisited, and the necessary modifications to apply it to three-dimensional elements are described. In particular, warping distortions vary depending on the cross-sectional geometry of the element, and thus a specific warping function for each geometry is proposed. Then, the effective warping rigidity and warping-related cross-sectional areas are derived for rectangular, circular and annular bearings following the assumptions of the pressure solution. Rubber compressibility is accounted for, but fiber extensibility is neglected based on results from previous studies on planar infinite strip bearings which indicate negligible impact of this parameter on their warping properties and stability (Pinarbasi and Mengi 2008, 2017; Montalto and Konstantinidis, "Buckling of short beams", submitted, *J. Eng. Mech.*, ASCE). The use of the cited buckling theory together with the derived warping properties is evaluated on the basis of a three-dimensional parametric finite element study for unbonded FREIs. Recommendations for the estimation of the buckling of FREIs are given and design resources are provided to aid the practical implementation of these results.

BUCKLING THEORY

Planar Formulation

The buckling of a planar beam accounting for nonuniform shear warping and axial shortening was presented in (Montalto and Konstantinidis, "Buckling of short beams", submitted, *J. Eng. Mech.*, ASCE). The beam with reference configuration $\mathcal{B} \subset \mathbb{R}^2$ such that $\mathcal{B} = \mathcal{A} \times [0, h]$, with cross section $\mathcal{A} \subset \mathbb{R}$ and height $h \subset \mathbb{R}$ is assumed to lie in the xz plane such that its line of centroids is aligned with the z axis in the undeformed configuration (see Fig. 1). Then, the beam deforms according to the displacement field $\mathbf{u}$ with x and z components given by:

$$u_x = v(z) \qquad u_z = \Delta(z) - x\psi(z) - f_w(x)\phi(z) \tag{2}$$

where $\Delta(z)$, $v(z)$ = the vertical and lateral displacements of the beam's axis, respectively, $\psi(z)$ = the cross-sectional rotation in the absence of warping, and $\phi(z)$ = the dimensionless amplitude multiplier for the cross-sectional warping $f_w(x)$.

The following conditions are enforced to decouple the generalized stress resultants P (axial load), M (bending moment), and Q (warping moment):

$$\int_{\mathcal{A}} f_w \sigma_\Delta(x)\, dA = 0 \qquad \int_{\mathcal{A}} f_w \sigma_\psi(x)\, dA = 0 \qquad \int_{\mathcal{A}} \sigma_\phi(x)\, dA = 0 \qquad \int_{\mathcal{A}} x\sigma_\phi(x)\, dA = 0 \tag{3}$$

where $\sigma_\Delta(x)$, $\sigma_\psi(x)$, $\sigma_\phi(x)$ = the axial stresses caused by an axial displacement, a rotation, and a warping deformation, respectively. These conditions impose restrictions on the definitions of the warping function $f_w(x)$. In the case of a homogeneous isotropic beam, such restrictions are:

$$\int_{\mathcal{A}} f_w(x)\, dA = 0 \qquad \int_{\mathcal{A}} x f_w(x)\, dA = 0 \tag{4}$$

which allow the interpretation of $\Delta(z)$ and $v(z)$ as the average axial and transverse displacements, respectively, and of $\psi(z)$ as the average rotation of the cross section.

Based on the previous displacement field and the assumption that stresses normal and tangent to the cross section are linear with respect to their work-conjugate strains, the following second-order accurate potential can be established for the beam:

$$\Pi(v,\psi,\phi) = \frac{1}{2}\int_0^h \begin{Bmatrix} \psi' \\ \phi' \\ \tilde{\gamma} \\ \tilde{\phi} \end{Bmatrix}^{\mathsf{T}} \begin{pmatrix} EI & 0 & 0 & 0 \\ 0 & EJ & 0 & 0 \\ 0 & 0 & GA+\tilde{P} & -GB-\tilde{P}\frac{f_B}{A} \\ 0 & 0 & -GB-\tilde{P}\frac{f_B}{A} & GC+\tilde{P}\frac{f_C}{A} \end{pmatrix} \begin{Bmatrix} \psi' \\ \phi' \\ \tilde{\gamma} \\ \tilde{\phi} \end{Bmatrix} - \tilde{P}(v')^2\, dz \tag{5}$$

where $\tilde{\gamma} = v' - \lambda_o\psi$, $\tilde{\phi} = \lambda_o\phi$, $\tilde{P} = P/\lambda_o$, and $\lambda_o = 1 - P/EA$ = the initial stretch of the beam due to the application of the axial load P. Moreover, EA, GA and EI correspond to the axial, shear and bending rigidities as normally defined, while EJ, B, C, f_B and f_C are the effective warping rigidity and warping-related areas dependent on the definition of the function f_w.

The equilibrium equations, shown in (Montalto and Konstantinidis, "Buckling of short beams", submitted, *J. Eng. Mech.*, ASCE), can be obtained by virtue of the principle of virtual work such that $\delta\Pi = 0$. These equations along with the appropriate boundary conditions are then used to obtain the critical load for the element. For a beam with fixed end conditions (i.e, no rotation or warping at the supports) but free to sway at the top, the normalized critical load $\bar{P}_{cr} = P_{cr}/GA$ corresponds to the solution of the following quartic equation:

$$\bar{P}\left\{\left[\bar{P}+\lambda_o(\bar{P})\right]\kappa_C(\bar{P})-\lambda_o(\bar{P})\,\kappa_B(\bar{P})\right\}+\pi^2\Omega\left\{\bar{P}\left[\bar{P}+\lambda_o(\bar{P})\right]+\kappa_B(\bar{P})-\kappa_C(\bar{P})\right\}-\pi^4\Omega^2=0 \qquad (6)$$

where $\Omega = EI/GAh^2$ is the bending-to-shear stiffness ratio, while $\lambda_o(\bar{P})$, $\kappa_B(\bar{P})$ and $\kappa_C(\bar{P})$ are:

$$\lambda_o(\bar{P}) = 1-\bar{P}\,\frac{GA}{EA} \qquad (7)$$

$$\kappa_B(\bar{P}) = \left(\bar{P}\,\frac{f_B}{A}+\lambda_o\,\frac{B}{A}\right)^2\frac{EI}{EJ} \qquad \kappa_C(\bar{P}) = \lambda_o\left(\bar{P}\,\frac{f_C}{A}+\lambda_o\,\frac{C}{A}\right)\frac{EI}{EJ} \qquad (8)$$

Hereinafter, Eq. (6) will be referred to as the *proposed-exact* equation.

Alternatively, the buckling load can be calculated from the approximate equation:

$$P_{cr} \approx \sqrt{\frac{P_S P_E}{1+\left(\frac{f_B}{A}\right)^2\frac{EI}{EJ}}} \qquad (9)$$

where $P_S = GA$ = shear rigidity, and $P_E = \pi^2 EI/h^2$ = Euler's buckling load. Haringx's buckling load [Eq. (1)] can be approximated by $P_{cr}^H \approx \sqrt{P_S P_E}$ when $P_E \gg P_S$. Then, Eq. (9) can be interpreted as this critical load reduced on the basis of the bending-to-warping rigidity ratio EI/EJ and the ratio f_B/A, which measures the angular deviation of the line of action of the axial load P with respect to the normal to the average cross-sectional plane. Eq. (9) was shown to predict critical loads very close to those of Eq. (6) for infinite strip bearings (Montalto and Konstantinidis, "Buckling of short beams", submitted, *J. Eng. Mech.*, ASCE). In the following, Eq. (9) will be referred to as the *proposed-approximate* equation.

Extension to Three-Dimensional Case

In the three-dimensional case, the beam has a cross section $\mathcal{A} \subset \mathbb{R}^2$, assumed to be doubly-symmetrical, such that its reference configuration $\mathcal{B} \subset \mathbb{R}^3$ is defined as $\mathcal{B} = \mathcal{A} \times [0, h]$. In the undeformed configuration, the cross section lies in the xy plane such that x and y correspond to the symmetry axis, while z is the centroidal axis as before. The lateral deformation is still assumed to occur in the xz plane, and the interpretation of the generalized displacements Δ, v, ψ and ϕ and the cross-sectional warping f_w remains the same. Again, the cross-sectional warping function satisfies the orthogonality conditions in Eq. (3) [or Eq. (4) for the homogeneous isotropic case]. The only difference is that f_w is now, in general, a function of both x and y. The definition of this cross-sectional warping function for a two-dimensional cross section is detailed next.

Warping function

In three-dimensional beam theories that consider cross-sectional warping (developed for numerical implementation), the warping function has often been taken as that from the solution to Saint-Venant's flexure problem with vanishing Poisson's ratio ν (El Fatmi 2007; Genoese et al. 2013; Dikaros and Sapountzakis 2014; Lewiński and Czarnecki 2021). This leads to formulations that account for out-of-plane cross-sectional warping but neglect in-plane cross-sectional distortion. In this study, this approach is adopted and the warping function is based on the so-called Saint-Venant warping. However, the latter function needs to be further modified to allow the axial load, the bending moment and the warping moment to be decoupled for the stress distribution that occurs in the bearings, which differs from that of homogeneous isotropic beams.

The Saint-Venant flexure problem consists of determining the three-dimensional linear elasticity solution to the problem of a cantilever beam subjected to tractions at its free end which are statically equivalent to a transverse load H acting through the centroid of the cross section. At the fixed end of the beam the centroidal displacement and a rotation are imposed to be zero, but no further essential boundary conditions are imposed. The traction boundary conditions at the free-end are specified in terms of the resultant transverse load H, while the point-wise tractions are assumed to be applied in such a way that they coincide with the stress distribution from the solution. Hence, this solution corresponds to that of unrestrained warping and end-effects are neglected. The problem has been solved in classic texts [e.g., Love (1944)] in terms of displacements for common cross-sectional geometries, including rectangular and circular ones.

The Saint-Venant warping function $f_w^{SV}(x,y)$ can be extracted from the exact displacement solutions presented, for example, by Love (1944) as shown in (Cowper 1966; Simo 1982). However, under the assumption of $\nu = 0$, a simpler approach can be adopted as illustrated next. The three-dimensional beam $\mathcal{B} \subset \mathbb{R}^3$ is defined as before with a height h and a cross section $\mathcal{A} \subset \mathbb{R}^2$ with boundary $\partial\mathcal{A}$ and normal vector $\mathbf{v}$, such that $\mathcal{B} = \mathcal{A} \times [0,h]$. In the undeformed configuration, the cross section lies in the xy plane, while the line of centroids of the beam is aligned with the z axis. The semi-fixed end is taken at $z = 0$, while tractions are applied at $z = h$ with a resultant H acting in the x direction through the centroid of the cross section. The cross-sectional boundary is traction-free throughout the beam such that $\boldsymbol{\sigma}\mathbf{v} = \mathbf{0}$ on $\partial\mathcal{A}$.

The exact displacement field for Saint-Venant's flexure problem with vanishing Poisson's ratio can be expressed as:

$$u_x = v(z) \qquad u_y = 0 \qquad u_z = -x\psi(z) - f_w^{SV}(x,y)[v'(z) - \psi(z)] \tag{10}$$

plus a rigid-body motion which depends on the specific rotation boundary condition enforced at the semi-fixed end $z = 0$. In this case, $v(z)$ and $\psi(z)$ have the same interpretation as before, being the average transverse displacement and average cross-sectional rotation respectively, while $f_w^{SV}(x,y)$ satisfies the orthogonality conditions in Eq. (4).

Defining the function $\Phi(x,y)$ as:

$$\Phi(x,y) = x - f_w^{SV}(x,y) \tag{11}$$

the strains can be written as:

$$\varepsilon_z = -\psi' x - f_w^{SV}(v'' - \psi') \qquad \gamma_{xz} = \Phi_{,x}(v' - \psi) \qquad \gamma_{yz} = \Phi_{,y}(v' - \psi) \tag{12}$$

with the rest of the strains being equal to zero; the notation $(\bullet)_{,x}$ represents the partial derivative with respect to x. For a homogeneous isotropic material with Young's modulus E and shear modulus G, the stresses are given by:

$$\sigma_z = -E[\psi' x + f_w^{SV}(v'' - \psi')] \qquad \tau_{xz} = G\Phi_{,x}(v' - \psi) \qquad \tau_{yz} = G\Phi_{,y}(v' - \psi) \tag{13}$$

Moreover, the traction-free boundary condition for the cross section now reads $\nabla\Phi \cdot \mathbf{v} = 0$ on $\partial\mathcal{A}$.

Neglecting body forces, the equations from the balance of linear momentum corresponding to $\mathrm{div}(\boldsymbol{\sigma}) \cdot \mathbf{e}_x = 0$ and $\mathrm{div}(\boldsymbol{\sigma}) \cdot \mathbf{e}_y = 0$ result in $(v'' - \psi') = 0$. Multiplying the last equilibrium equation $\mathrm{div}(\boldsymbol{\sigma}) \cdot \mathbf{e}_z = 0$ by x, integrating over the cross section and making use of $\boldsymbol{\sigma}\mathbf{v} = \mathbf{0}$ on $\partial\mathcal{A}$, the relation $-EI\psi'' = \kappa GA(v' - \psi)$ is recovered, where κ has been defined as:

$$\kappa = \frac{\int_{\mathcal{A}} \Phi_{,x}\, dA}{A} \tag{14}$$

Using this relation in $\mathrm{div}(\boldsymbol{\sigma}) \cdot \mathbf{e}_z = 0$, the following is obtained:

$$\nabla^2\Phi + \frac{\kappa A}{I} x = 0 \tag{15}$$

The Saint-Venant warping function can be determined by solving the elliptic problem in Eq. (15) over the cross section $\mathcal{A}$, with the traction boundary condition $\nabla\Phi \cdot \mathbf{v} = 0$ on $\partial\mathcal{A}$ and the relation $f_w^{SV} = x - \Phi$. Additionally, the orthogonality conditions in Eq. (4) need to be enforced to uniquely define the solution. Following this approach, the Saint-Venant warping function is obtained for a rectangular cross section with width $2b$ in the x direction and depth $2l$ in the y direction:

$$f_w^{SV}(x, y) = \frac{5}{6}\left(\frac{x^3}{2b^2} - \frac{3}{10}x\right) \tag{16}$$

For the circular and annular cross sections, we make use of polar coordinates such that $x = r\cos(\theta)$ and $y = r\sin(\theta)$. Then, the warping function for these cross sections is given by:

$$f_w^{SV}(r, \theta) = \frac{\kappa}{1 + \eta^2}\left[\frac{r^3}{2b^2} + \left(\frac{1}{\kappa} - \frac{3}{2}\right)(1 + \eta^2)r - \frac{3\eta^2 b^2}{2r}\right]\cos(\theta), \qquad \kappa = \frac{6(1 + \eta^2)^2}{7 + 34\eta^2 + 7\eta^4} \tag{17}$$

where b = the exterior radius of the cross section, a = the interior radius, and $\eta = a/b$ = the interior-to-exterior radius ratio; for a circular cross section $\eta = 0$.

Enforcing the orthogonality conditions in Eq. (4) allows to decouple the generalized stress resultants P, M and Q in the case of an isotropic homogeneous beam. However, for an elastomeric bearing the stress distributions are not proportional to the cross-sectional deformations, and thus the general conditions in Eq. (3) are required. The Saint-Venant warping functions are then modified to allow the satisfaction of these requirements. For the rectangular case we use:

$$f_w(x, y) = \frac{5}{6}\left(\frac{x^3}{2b^2} + \omega x\right) \tag{18}$$

For the circular and annular cross sections we have:

$$f_w(r, \theta) = \frac{6}{7}\left(\frac{r^3}{2b^2} + \omega r - \frac{3\eta^2 b^2}{2r}\right)\cos(\theta) \tag{19}$$

where ω is a parameter that depends on the cross section and material properties, which is obtained from the satisfaction of Eq. (3). These warping functions are shown in Fig. 2.

EFFECTIVE WARPING PROPERTIES

Whereas the buckling theory assumes a homogeneous isotropic material in the element, the mechanical response of an elastomeric isolator is governed by the composite action of the rubber and the reinforcement, producing different stress distributions than those obtained by the beam theory. *Effective* rigidities are thus required to apply the buckling theory to elastomeric isolators; see discussion following Eq. (1) for the analogous case of using Haringx's theory for SREIs. The effective axial and bending rigidities, $\widetilde{EA}$ and $\widetilde{EI}$, considering rubber compressibility but not reinforcement extensibility have already been presented for different bearing geometries by Kelly and Konstantinidis (2011). In the following, the effective warping-related properties for bearings with rectangular, circular and annular cross section are derived.

Boundary Value Problem

The effective rigidites are obtained by evaluating the mechanical response of a single rubber layer of thickness t_e using linear elasticity and following traditional assumptions regarding the deformation of the layer and the stress distribution (Kelly and Konstantinidis 2011). Namely, it is assumed that vertical lines are deformed into a parabola, and that the vertical displacement varies linearly throughout the layer. Furthermore, it is assumed that the normal stresses are dominated by the internal pressure p such that $\sigma_x \approx \sigma_y \approx \sigma_z \approx -p$, while the in-plane shear stress $\tau_{xy} \approx 0$. This leads to the so-called *pressure solution* (Gent and Lindley 1959; Gent and Meinecke 1970; Kelly and Konstantinidis 2011). These assumptions have been shown to be accurate for layers of nearly incompressible material bonded to nearly inextensible reinforcement when the shape factors S (i.e., ratio of loaded to force-free area) are in the typical range used in elastomeric isolators (10 - 30) using more refined analytical solutions (Papoulia and Kelly 1996; Pinarbasi and Mengi 2008).

Pinarbasi and Mengi (2008, 2017) showed that, for layers of nearly incompressible material with high shape factor bonded to reinforcement with axial rigidity values characteristic of the fiber in FREIs, reinforcement extensibility has a negligible influence on the effective warping rigidity of infinite strip bearings. Moreover, results in (Montalto and Konstantinidis, "Buckling of short beams", submitted, *J. Eng. Mech.*, ASCE) indicated that reinforcement extensibility has a negligible effect in the buckling of planar infinite strip bearings considering realistic material parameters and thickness of the fiber. Reinforcement extensibility is measured by the dimensionless parameter $\alpha \propto \sqrt{Gt_e/E_f t_f}\,S$, where E_f = fiber Young's modulus, and t_f = fiber thickness, while rubber compressibility is measured by the dimensionless parameter $\beta \propto \sqrt{G/K}\,S$, where K = rubber bulk modulus (Van Engelen et al. 2016). For a given shape factor S, the required thickness t_e of a three-dimensional layer is smaller than that of its planar counterpart. Thus, α is reduced while β remains the same and the influence of fiber extensibility is expected to be even lower in three-dimensional bearings. Therefore, the following analysis will account for rubber compressibility but neglect the extensibility of the fiber reinforcement.

Following the presentation for the beam theory, it is assumed that the isolator's axis is oriented along the z direction with the mid-height of the layer located at $z = 0$, while the reinforcement lies in the xy plane (see Fig. 3). Then, the assumed displacement field is as follows:

$$u(\mathbf{x}) = u_0(x,y)\left(1 - \frac{4z^2}{t_e^2}\right) \qquad v(\mathbf{x}) = v_0(x,y)\left(1 - \frac{4z^2}{t_e^2}\right) \qquad w(\mathbf{x}) = -f_w(x,y)\phi\frac{z}{t_e} \tag{20}$$

where $u(\mathbf{x})$, $v(\mathbf{x})$ and $w(\mathbf{x})$ are the displacement fields in the x, y and z directions respectively, and $u_0(x,y)$ and $v_0(x,y)$ are functions to be determined based on the solution to the boundary-value problem. As indicated before, it is assumed that the displacement along the axis of the beam varies linearly. Hence, $\phi/2$ corresponds to the warping amplitude at the top and bottom of the layer, while the term z/t_e provides the linear variation of the displacement explicitly. The warping function $f_w(x,y)$ depends on the cross-sectional geometry and is given by Eq. (18) for the rectangular case, and Eq. (19) for the circular and annular ones. The corresponding strain fields for the rubber are:

$$\varepsilon_x(\mathbf{x}) = u_{0,x}\left(1 - \frac{4z^2}{t_e^2}\right) \qquad \varepsilon_y(\mathbf{x}) = v_{0,y}\left(1 - \frac{4z^2}{t_e^2}\right) \qquad \varepsilon_z(\mathbf{x}) = -f_w\frac{\phi}{t_e} \tag{21}$$

$$\gamma_{xz}(\mathbf{x}) = -\left(\frac{8u_0}{t_e} + f_{w,x}\phi\right)\frac{z}{t_e} \qquad \gamma_{yz}(\mathbf{x}) = -\left(\frac{8v_0}{t_e} + f_{w,y}\phi\right)\frac{z}{t_e} \tag{22}$$

The material constitutive relation for the volumetric deformation of the rubber is given by $\mathrm{tr}(\boldsymbol{\varepsilon}) = -p(x,y)/K$, where K = bulk modulus of the rubber, leading to the equation:

$$\left(u_{0,x} + v_{0,y}\right)\left(1 - \frac{4z^2}{t_e^2}\right) - f_w\frac{\phi}{t_e} = -\frac{p}{K} \tag{23}$$

Integrating this equation through the thickness of the rubber layer, we obtain:

$$\frac{2}{3}\left(u_{0,x} + v_{0,y}\right) - f_w\frac{\phi}{t_e} = -\frac{p}{K} \tag{24}$$

The shear stresses are obtained from the material constitutive relation:

$$\tau_{xz}(\mathbf{x}) = -G\left(\frac{8u_0}{t_e} + f_{w,x}\phi\right)\frac{z}{t_e} \qquad \tau_{yz}(\mathbf{x}) = -G\left(\frac{8v_0}{t_e} + f_{w,y}\phi\right)\frac{z}{t_e} \tag{25}$$

where G = shear modulus of the rubber.

Now we make use of the balance of linear momentum for the rubber layer, which in the absence of body forces and under quasi-static conditions reads $\mathrm{div}(\boldsymbol{\sigma}) = \mathbf{0}$. Under the assumptions that the normal stresses are dominated by the pressure and that τ_{xy} is negligible in comparison to the other stress components, the first equation of equilibrium, corresponding to $\mathrm{div}(\boldsymbol{\sigma}) \cdot \mathbf{e}_x = 0$, results in:

$$p_{,x} + \frac{G}{t_e}\left(\frac{8u_0}{t_e} + f_{w,x}\phi\right) = 0 \tag{26}$$

The second equilibrium equation, corresponding to $\mathrm{div}(\boldsymbol{\sigma}) \cdot \mathbf{e}_y = 0$, becomes:

$$p_{,y} + \frac{G}{t_e}\left(\frac{8v_0}{t_e} + f_{w,y}\phi\right) = 0 \tag{27}$$

Taking the partial derivative of Eq. (26) with respect to x, the partial derivative of Eq. (27) with respect to y, adding them together, and substituting $u_{0,x} + v_{0,y}$ using Eq. (24), we obtain the following equation for the pressure $p(x, y)$:

$$\nabla^2 p - \left(\frac{12G}{Kt_e^2}\right) p = -\frac{12G\phi}{t_e^3}\left(f_w + \frac{t_e^2}{12}\nabla^2 f_w\right) \tag{28}$$

For rubber layers with a shape factor S in the range used for elastomeric isolators (10-30), the last term in the parenthesis of the right-hand side of the pressure equation is at least a couple of orders of magnitude smaller than the leading terms and is thus neglected in the following.

The pressure distribution on the layer due to a warping deformation is obtained from Eq. (28), alongside the boundary condition $p = 0$ on the cross-sectional boundary. This pressure distribution is then used to determine the effective warping rigidity and warping-related areas, following their definitions given in (Montalto and Konstantinidis, "Buckling of short beams", submitted, *J. Eng. Mech.*, ASCE), recalling that the warping displacement has been assumed to vary linearly in the rubber layer such that $\phi' = \phi/t_e$ and taking $P/A = (\Delta/t_e)(\widetilde{EA}/A)$:

$$\widetilde{EJ} = \frac{\int_{\mathcal{A}} f_w p dA}{\phi/t_e} \tag{29}$$

$$B = \int_{\mathcal{A}} f_{w,x} dA \qquad C = \int_{\mathcal{A}} (f_{w,x})^2 \, dA \tag{30}$$

$$f_B = \frac{A \int_{\mathcal{A}} f_{w,x} p_\Delta dA}{(\Delta/t_e)\widetilde{EA}} \qquad f_C = \frac{A \int_{\mathcal{A}} (f_{w,x})^2 \, p_\Delta dA}{(\Delta/t_e)\widetilde{EA}} \tag{31}$$

where p_Δ = pressure due to an axial shortening displacement Δ, and $\widetilde{EA}$ = effective axial rigidity.

Rectangular Layer

For the case of a rectangular cross section, we consider the layer to have a width of $2b$ in the x direction and a depth of $2l$ in the y direction. Therefore, the shape factor is given by:

$$S = \frac{bl}{(b+l)\,t_e} = \frac{b}{t_e}\frac{1}{(1+\rho)} \tag{32}$$

where $\rho = b/l$ gives the in-plane aspect ratio of the bearing. Making use of the warping function in Eq. (18), the partial differential equation for the pressure can be restated as:

$$p_{,xx} + p_{,yy} - \left(\frac{\beta}{b}\right)^2 p = -\frac{10G\phi}{t_e^3}\left(\frac{x^3}{2b^2} + \omega x\right) \tag{33}$$

where,

$$\beta^2 = \frac{12Gb^2}{Kt_e^2} = \frac{12G}{K} S^2 (1+\rho)^2 \tag{34}$$

The solution to Eq. (33) is obtained by assuming a single Fourier series in the x direction. The resulting pressure is given by:

$$p(x,y) = 10GS^2(1+\rho)^2 \left(\frac{b\phi}{t_e}\right) \sum_{n=1}^{\infty} \frac{(-1)^n[6 - n^2\pi^2(1+2\omega)]}{\xi_n^2 n^3 \pi^3} \left[1 - \frac{\cosh(\xi_n y/b)}{\cosh(\xi_n/\rho)}\right] \sin\left(\frac{n\pi x}{b}\right) \tag{35}$$

where $\xi_n^2 = (n\pi)^2 + \beta^2$. The parameter ω is obtained using Eq. (3). Albeit not shown here for brevity, the first two conditions are analogous to the third and fourth conditions, and the latter two are used. The third condition is trivially satisfied. The fourth condition yields:

$$\sum_{n=1}^{\infty} \frac{n^2\pi^2(1+2\omega)-6}{n^4\pi^4\xi_n^2}\left[1-\frac{\tanh(\xi_n/\rho)}{\xi_n/\rho}\right]=0 \tag{36}$$

Because the pressure in the rectangular layer is given in terms of an infinite Fourier series, the orthogonality condition for the warping function does not have a closed-form solution for ω; hence Eq. (36) requires to be solved numerically. In general, it depends on the ratio K/G, the in-plane aspect ratio ρ and the shape factor S. Numerical results for this are presented in Fig. 4.

The effective warping rigidity $\widetilde{EJ}$ and the cross-sectional areas B and C can then be obtained from their definitions in Eqs. (29) and (30):

$$\widetilde{EJ} = \frac{50}{3}\frac{GS^2(1+\rho)^2b^4}{\rho}\sum_{n=1}^{\infty}\frac{\left[n^2\pi^2(1+2\omega)-6\right]^2}{n^6\pi^6\xi_n^2}\left[1-\frac{\tanh(\xi_n/\rho)}{\xi_n/\rho}\right] \tag{37}$$

$$B = \frac{5b^2}{3\rho}(1+2\omega) \tag{38}$$

$$C = \frac{5b^2}{36\rho}(9+20\omega+20\omega^2) \tag{39}$$

For the calculation of the areas f_B and f_C, the pressure due to a vertical displacement Δ, denoted p_Δ, is required. This has been presented by Kelly and Konstantinidis (2011) accounting for rubber compressibility. When the origin of the Cartesian system is located at the centroid of the layer, this pressure is given by:

$$p_\Delta(x,y) = 48GS^2(1+\rho)^2\left(\frac{\Delta}{t_e}\right)\sum_{n=1}^{\infty}\frac{(-1)^n}{\zeta_n^2(2n-1)\pi}\left[1-\frac{\cosh(\zeta_n y/b)}{\cosh(\zeta_n/\rho)}\right]\cos\left[\frac{(2n-1)\pi x}{2b}\right] \tag{40}$$

where $\zeta_n^2 = \left[(2n-1)\pi/2\right]^2+\beta^2$. The effective axial rigidity $\widetilde{EA}$ is given by:

$$\widetilde{EA} = \frac{384GS^2(1+\rho)^2b^2}{\rho}\sum_{n=1}^{\infty}\frac{1}{\zeta_n^2(1-2n)^2\pi^2}\left[1-\frac{\tanh(\zeta_n/\rho)}{\zeta_n/\rho}\right] \tag{41}$$

Using Eq. (31), the areas f_B and f_C are given by:

$$f_B = \frac{5b^2}{3\rho} \frac{\sum_{n=1}^{\infty} \frac{[-24+(1-2n)^2\pi^2(3+2\omega)]}{\zeta_n^2(1-2n)^4\pi^4} \left\{1 - \frac{\tanh(\zeta_n/\rho)}{\zeta_n/\rho}\right\}}{\sum_{n=1}^{\infty} \frac{1}{\zeta_n^2(1-2n)^2\pi^2} \left\{1 - \frac{\tanh(\zeta_n/\rho)}{\zeta_n/\rho}\right\}} \tag{42}$$

$$f_C = \frac{25b^2}{36\rho} \frac{\sum_{n=1}^{\infty} \frac{[3456+(1-2n)^4\pi^4(3+2\omega)^2-48(1-2n)^2\pi^2(9+2\omega)]}{\zeta_n^2(1-2n)^6\pi^6} \left\{1 - \frac{\tanh(\zeta_n/\rho)}{\zeta_n/\rho}\right\}}{\sum_{n=1}^{\infty} \frac{1}{\zeta_n^2(1-2n)^2\pi^2} \left\{1 - \frac{\tanh(\zeta_n/\rho)}{\zeta_n/\rho}\right\}} \tag{43}$$

The previous results provide all the warping related properties needed for the estimation of the buckling load. However, the effective bending rigidity $\widetilde{EI}$ is also required. Accounting for rubber compressibility, this is given by (Kelly and Konstantinidis 2011):

$$\widetilde{EI} = \frac{96GS^2(1+\rho)^2b^4}{\rho} \sum_{n=1}^{\infty} \frac{1}{n^2\pi^2\xi_n^2} \left[1 - \frac{\tanh(\xi_n/\rho)}{\xi_n/\rho}\right] \tag{44}$$

The critical load for the bearing can then be computed using Eqs. (6) or (9) with the previous effective cross-sectional properties. Fig. 5 presents the comparison between the critical load estimates of these equations as a function of the shape factor S and the width-to-height aspect ratio $S_2^* = 2b/h$. These results verify that the proposed-approximate solution [Eq. (9)] provides close estimates to those of Eq. (6) for the isolator with rectangular cross section.

Circular and Annular Layers

For the circular and annular cases, we consider the layer to have an exterior radius of b, an interior radius a, and an interior-to-exterior radius ratio $\eta = a/b$; for circular cross sections $\eta = 0$. Hence, the shape factor is given by:

$$S = \frac{b-a}{2t_e} = \frac{b(1-\eta)}{2t_e} \tag{45}$$

In this case the warping function is given by Eq. (19). Then, the partial differential equation for the pressure [Eq. (28)] in polar coordinates becomes:

$$p_{,rr} + \frac{1}{r}p_{,r} + \frac{1}{r^2}p_{,\theta\theta} - \left(\frac{\beta}{b}\right)^2 p = -\frac{72G\phi}{7t_e^3}\left(\frac{r^3}{2b^2} + \omega r - \frac{3\eta^2 b^2}{2r}\right)\cos(\theta) \tag{46}$$

where the non-dimensional ratio β measuring the compressibility of the material corresponds to:

$$\beta^2 = \frac{12Gb^2}{Kt_e^2} = \frac{48GS^2}{K(1-\eta)^2} \tag{47}$$

Circular Layer

For the circular layer, the solution to Eq. (46) is given in terms of modified Bessel functions of the first kind of order m, referenced as $I_m(r)$:

$$p(r,\theta) = \frac{144GS^2}{7\beta^2}\left(\frac{b\phi}{t_e}\right)\left\{\left(\frac{r}{b}\right)^3 + 2\left(\frac{r}{b}\right)\left(\frac{4}{\beta^2} + \omega\right) - \frac{[1 + 2(4/\beta^2 + \omega)]I_1(\beta r/b)}{I_1(\beta)}\right\}\cos(\theta) \tag{48}$$

As before, the parameter ω defining the warping function $f_w(r,\theta)$ is calculated from satisfying the third and fourth orthogonality conditions in Eq. (3) (equivalent to the first two conditions). The third orthogonality condition is directly satisfied. Then, the fourth orthogonality condition is used to determine ω, and the following is obtained:

$$\omega = \frac{-\beta(12+\beta^2)I_1(\beta) + 6(8+\beta^2)I_2(\beta)}{3\beta^3 I_3(\beta)} \tag{49}$$

The warping properties are then obtained following the same approach as for the rectangular layer. Using Eq. (29), the effective warping rigidity is given by:

$$\widetilde{EJ} = \frac{18\pi GS^2 b^4}{49\beta^2}\left\{3 + 8\omega(2+3\omega) + \frac{16(5+12\omega)}{\beta^2} + \frac{384}{\beta^4} - \frac{24[8+\beta^2(1+2\omega)]^2 I_2(\beta)}{\beta^5 I_1(\beta)}\right\} \tag{50}$$

The areas B and C are calculated from Eq. (30):

$$B = \frac{3}{7}\pi b^2(1 + 2\omega) \tag{51}$$

$$C = \frac{9}{98}\pi b^2(3 + 8\omega + 8\omega^2) \tag{52}$$

The calculation of the areas f_B and f_C requires the pressure p_Δ. When accounting for rubber compressibility, this corresponds to (Kelly and Konstantinidis 2011):

$$p_\Delta(r, \theta) = \frac{48GS^2}{\beta^2}\left(\frac{\Delta}{t}\right)\left[1 - \frac{I_0(\beta r/b)}{I_0(\beta)}\right] \tag{53}$$

The effective axial rigidity $\widetilde{EA}$ for the circular cross section is:

$$\widetilde{EA} = \frac{48\pi GS^2 b^2}{\beta^2}\frac{I_2(\beta)}{I_0(\beta)} \tag{54}$$

Hence, the areas f_B and f_C [Eq. (31)] are given by:

$$f_B = \frac{3}{7}\pi b^2\left\{\frac{\beta[8 + \beta^2(1 + 2\omega)]I_0(\beta) - 4[4 + \beta^2(1 + \omega)]I_1(\beta)}{\beta^3 I_2(\beta)}\right\} \tag{55}$$

$$\begin{aligned} f_C = \frac{9}{98}\pi b^2 \Bigg\{ & \frac{\beta\left\{576 + 8\beta^2(9 + 8\omega) + \beta^4[3 + 8\omega(1 + \omega)]\right\}I_0(\beta)}{\beta^5 I_2(\beta)} \\ & - \frac{2\left\{576 + 16\beta^2(9 + 4\omega) + \beta^4[9 + 8\omega(2 + \omega)]\right\}I_1(\beta)}{\beta^5 I_2(\beta)}\Bigg\} \end{aligned} \tag{56}$$

Similar to the case of the rectangular bearings, it is convenient to provide the effective bending rigidity, which corresponds to (Kelly and Konstantinidis 2011):

$$\widetilde{EI} = \frac{48\pi b^4 GS^2}{\beta^2}\left[\frac{1}{4} - \frac{I_2(\beta)}{\beta I_1(\beta)}\right] \tag{57}$$

Then, the critical load for the bearing can be computed using the proposed-exact expression [Eq.

(6)] or the proposed-approximate closed-form solution [Eq. (9)] with the effective cross-sectional properties presented before. Fig. 6 shows that Eq. (9) provides excellent agreement with Eq. (6) for the circular bearing. In this figure results are presented in terms of the shape factor S and the width-to-height aspect ratio $S_2^* = 2b/h$.

Annular Layer

Albeit common in the context of SREIs, annular FREIs have seldom been explored. Only recently have they been evaluated with the purpose of isolating lightweight structures and nonstructural components (Ghorbi and Toopchi-Nezhad 2023). Because of this and the length and complexity of the resulting equations, the corresponding effective warping rigidity and warping-related cross-sectional properties are presented in Appendix I for the interested reader. Using these properties, Fig. 6 shows the excellent agreement between Eqs. (6) and (9) for the critical load estimation of annular bearings.

Kelly and Konstantinidis (2011) recognized that, when warping is neglected, the introduction of an inner hole in the bearing causes a negligible reduction in the critical pressure $p_{cr} = P_{cr}/A$, and the reduction in the critical load is approximately of the same proportion as the area reduction. However, this is not the case when warping occurs, as illustrated in Fig. 7, where the critical pressure of an annular bearing has been normalized by that of a circular bearing with the same outer radius and layer thickness. When neglecting warping, an inner hole with $\eta = 0.40$ reduces p_{cr} by no more than 15%, while the reduction for smaller holes is negligible. In contrast, when accounting for warping using Eq. (6) and the properties in Appendix I, even a small hole with $\eta = 0.1$ reduces p_{cr} as much as 35%, while for $\eta = 0.4$ this reduction is greater than 70% in some cases. Note that the critical load P_{cr} is reduced even further due to the area reduction.

FINITE ELEMENT ANALYSIS

The use of the proposed effective warping properties and Eq. (9) was validated by a finite element parametric study developed using the nonlinear FEA software `Marc` (Hexagon AB 2021a). Isolators with rectangular, circular and annular cross sections were modeled in an unbonded configuration, and the critical load estimates from the numerical models were used as a benchmark to evaluate the analytical formulation. In the following, the modeling and results are described.

Modeling

To avoid volumetric locking and element failure due to mesh distortions, mixed-formulation low-order elements were used for the rubber. A three-field formulation proposed by Simo et al. (1985) was used; it is derived from a variational principle using the following functional:

$$\Pi(\boldsymbol{\varphi}, p, \theta) = \int_{\mathcal{B}} \left[\hat{W}(\hat{\mathbf{C}}) + U(\theta) + p\,(J - \theta) \right] dV + \Pi_{ext}(\boldsymbol{\varphi}) \tag{58}$$

where the fields are $\boldsymbol{\varphi}$ = deformation, p = pressure, and θ = volumetric strain. Additionally, $J = \det(\mathbf{F})$, where $\mathbf{F} = \partial\boldsymbol{\varphi}/\partial\mathbf{X}$ = the deformation gradient, and $\Pi_{ext}(\boldsymbol{\varphi})$ = the external potential energy due to the imposed body forces and surface tractions; $\hat{W}(\hat{\mathbf{C}})$ and $U(\theta)$ are defined in the following. The functional $\Pi(\boldsymbol{\varphi}, p, \theta)$ uses the multiplicative split of $\mathbf{F}$ given by:

$$\bar{\mathbf{F}} = \theta^{1/3}\,\hat{\mathbf{F}}, \tag{59}$$

where $\hat{\mathbf{F}} = J^{-1/3}\,\mathbf{F}$ = isochoric part of $\mathbf{F}$. The domains were discretized using Q1-P0 hexahedral elements, which use continuous piecewise trilinear interpolation for the deformation field and piecewise constant interpolation for the pressure and volumetric strain fields (Simo et al. 1985); this corresponds to element type 7 in `Marc` with the constant dilation parameter activated (Hexagon AB 2021b). They were implemented in an Updated Lagrangian formulation.

An additive split of the strain energy $W(\bar{\mathbf{C}}) = \hat{W}(\hat{\mathbf{C}}) + U(\theta)$ has been assumed in Eq. (58), where $\hat{W}$ and U are the deviatoric and volumetric parts of the strain energy, respectively, and $\hat{\mathbf{C}} = \hat{\mathbf{F}}^T\hat{\mathbf{F}}$ is the modified right Cauchy-Green deformation tensor. A compressible neo-Hookean model was used for the rubber, whose corresponding deviatoric strain energy defined by the shear modulus G and bulk modulus K is given by:

$$\hat{W}(\hat{\mathbf{C}}) = \frac{G}{2}\,(I_{\hat{\mathbf{C}}} - 3) \tag{60}$$

where $I_{\hat{\mathbf{C}}} = \mathrm{tr}(\hat{\mathbf{C}})$. This model is considered to represent rubber response accurately in the small to moderate deformation range (principal stretches in the range of 0.5-2.0) (Treloar 2005; Steigmann 2017), which covers the range of deformation exhibited in the numerical simulations. The following volumetric strain energy satisfying polyconvexity and growth conditions was used:

$$U(\theta) = K\left(\frac{\theta^2 - 1}{4} - \frac{\ln\theta}{2}\right) \tag{61}$$

Only half of each isolator was modeled considering symmetry conditions (see Fig. 8); for the nodes lying on the plane of symmetry, no displacement was allowed perpendicular to such plane. Three elements were used along the height of each rubber layer. For the isolators with rectangular cross section, a structured mesh was applied using transfinite interpolation such that a coarser mesh with element width-to-height aspect ratios of approximately 4:1 was produced at the interior of the bearing, and a finer mesh was produced towards the edges. In the case of the circular and annular isolators, a two-dimensional unstructured mesh was produced over the cross section using `Marc`'s `MoM` mesh generator (Hexagon AB 2021a); this planar mesh was later extruded to produce a structured mesh over the height of the bearing. In this case, the width-to-height aspect ratio of the elements was maintained at 2:1 over the entire bearing. These mesh sizes were verified to achieve convergence of the estimated critical loads.

The fiber reinforcement was modeled using quadrilateral membrane elements in a Total Lagrangian formulation; this corresponds to element type 18 in `Marc` (Hexagon AB 2021b). These elements use bilinear displacement interpolation and have no flexural rigidity. Moreover, they have zero out-of-plane thickness and therefore the overall height-to-total rubber thickness ratio $h/t_r = 1$ in the models. The fiber reinforcement material is modeled as linear elastic, defined by its Young's modulus E_f and Poisson's ratio ν_f. The contact between the bearing and its supports and the bearing with itself was modeled with a node-to-segment formulation, where the top and bottom supports were represented by rigid planar surfaces. Coulomb friction was used to model the friction between isolator and its supports with a friction coefficient $\mu = 1$.

Buckling Analysis Method

The isolator model was progressively loaded by a compressive axial load P in the range of 0.5 to 1.5 times the critical load estimated by Eq. (9). After every ramp load increment of 5%, the axial load was held constant while a small lateral perturbation was applied to the model (see Fig. 9a). This perturbation corresponded to a maximum lateral displacement u_{xo} of 0.2 mm at the top support, inducing an average shear strain of 0.2% in the isolator. Based on this, the global lateral stiffness of the isolator K_h was measured at different axial loads. The buckling load was taken as the axial load at which K_h vanishes (see Fig. 9b).

Cases

The variable parameters in the study were the shape factor S, the width-to-height aspect ratio S_2^*, the in-plane aspect ratio ρ for rectangular isolators, and the interior-to-exterior radius ratio η for circular and annular isolators. The values for these parameters included in the analysis are presented in Table 1; the values presented for S_2^* are satisfied exactly, while reported S are target values and the actual values of the models differ slightly from those in Table 1. All the combinations between these parameters were considered, except those leading to less than 5 or more than 25 rubber layers which were deemed unrealistic for practical scenarios. Hence, a total of 100 cases were evaluated, 50 of which were bearings with rectangular cross section and the remaining ones with circular or annular cross section. In all the analyses the bearing height was fixed at 100 mm, the rubber was modeled with a shear modulus $G = 0.4$ MPa and bulk modulus $K = 2000$ MPa, while the fiber reinforcement was modeled with a fiber thickness $t_f = 0.5$ mm, Young's modulus $E_f = 100000$ MPa, and Poisson's ratio $\nu_f = 0.20$.

Results

The FEA results are used as a benchmark to study the adequacy of the buckling theory and the effective warping properties derived herein. Figs. 10 and 11 present the critical loads estimated with the proposed-approximate formulation [Eq. (9)] normalized by the critical loads from the FEA models. As can be interpreted from Figs. 5 and 6, the results for the proposed-exact formulation are nearly identical to those of Eq. (9), and hence are not presented in the following. Figures 10 and 11 also present the critical loads estimated using Haringx's theory for comparison purposes. The estimates using the proposed-approximate equation and Haringx's theory have both used the effective properties accounting for rubber compressibility, but not fiber extensibility.

Figures 10 and 11 show that the proposed-approximate formulation exhibits excellent agreement with the results obtained from the FEA models. The critical loads tend to be slightly underestimated by the proposed formulation when the isolators have low shape factors S, associated with higher compressibility. Similar findings were shown for the planar bearings in (Montalto and Konstantinidis, "Buckling of short beams", submitted, *J. Eng. Mech.*, ASCE), where it was explained how bearings with low S experience larger vertical deformation and lateral expansion before buckling, leading to an increase in cross-sectional dimensions that increases their critical load; this is not accounted for by the one-dimensional buckling formulation. However, the cross-sectional expansion in the three-dimensional isolators occurs in two-directions and thus has a less significant effect in the results than for the planar infinite strip bearings. Therefore, the proposed-approximate formulation presents a better performance for the three-dimensional bearings than the planar ones, for which it was already satisfactory.

In contrast, Figs. 10 and 11 show that Haringx's theory can severely overestimate the buckling load of FREIs. This overestimation was in the range of 1.35 - 2.0 times the critical load obtained from the FEA models for rectangular isolators, and in the range of 1.35 - 1.75 for circular ones, with the error increasing with the shape factor S. For annular bearings the overprediction is greater and, for the cases evaluated, lies between 2.0 - 3.0 times the P_{cr} from the FEA models. The error increases again with S but also increases significantly with the relative size of the inner hole measured by η; this is in agreement with results presented in Fig. 7. In the case of SREIs, the introduction of an inner hole in a circular bearing has a negligible effect on its stability (Kelly and Konstantinidis 2011). However, this is not the case for FREIs. Despite not being evaluated here, it is expected that the introduction of a hole on rectangular FREIs would yield similar results. Interior holes in FREIs have been proposed to reduce the isolator lateral stiffness for applications dealing with lightweight structures (Van Engelen et al. 2014; Osgooei et al. 2015; Ghorbi and Toopchi-

Nezhad 2023). It is recognized that, despite the severe reduction in critical load, stability might not be an issue in those cases. However, the impact of compressive loads on the lateral behavior can be significant as the axial load will be much closer to the critical load than formerly expected.

RECOMMENDATIONS FOR DESIGN

Based on the results from the finite element analysis, the buckling theory presented in (Montalto and Konstantinidis, "Buckling of short beams", submitted, *J. Eng. Mech.*, ASCE) along with the effective warping properties derived herein produce an adequate estimation of the critical load for FREIs. Therefore, it is recommended that either Eq. (6) or Eq. (9) be used to evaluate the stability of FREIs. The latter, however, is deemed more useful for practical application purposes due to its simplicity. Rubber compressibility should be accounted for in the calculation of the effective rigidities, especially for bearings with moderate-to-high shape factor S. Alternatively, the buckling load accounting for warping can be presented as:

$$P_{cr} = \frac{P_{cr}^{H}}{f_R} \tag{62}$$

where P_{cr}^{H} is the critical load due to Haringx's theory given by Eq. (1). This reduction factor has been computed using Eq. (6) for different geometric and material parameters, and is presented in Figs. 12 and 13 for practical implementation of these results.

It should be noted that $h/t_r = 1$ has been assumed thus far due to the negligible fiber thickness t_f in comparison to the rubber thickness of a single layer t_e for typical FREIs. However, for some bearing configurations with very thin rubber layers, this might not hold. For SREIs the approach has been to increase the effective rigidities of a single layer (e.g., GA, $\widetilde{EI}$, $\widetilde{EJ}$) by the factor h/t_r (Gent 1964; Kelly and Konstantinidis 2011); see discussion following Eq. (1). Following this approach, effective rigidities for the multilayer bearing [e.g., $\widetilde{EI}_b = \widetilde{EI}(h/t_r)$] should be used in Eqs. (6) and (9). Alternatively, Eq. (9) shows that this simply leads to an amplification factor of h/t_r for P_{cr} calculated using the effective rigidities of a single layer presented before, and this approach is recommended due to the multiple effective properties required in Eqs. (6) or (9). The detailed calculation of the effective warping properties and buckling load for each of the bearing geometries presented in this study is illustrated in Appendix II.

CONCLUSIONS

This study investigated the warping of three-dimensional FREIs and its impact on their buckling load P_{cr}. First, modifications necessary to apply the planar buckling theory accounting for shear warping previously presented by the authors were described. In particular, warping functions were introduced for each of the evaluated cross sections by modifying the warping displacements from the Saint-Venant flexure problem to allow for decoupling of the generalized stress resultants in the isolators. Then, effective warping properties were derived for rectangular, circular and annular isolators, following the usual assumptions from the *pressure solution*. In these derivations, the effect of rubber compressibility was included but fiber extensibility was neglected because previous studies noted the latter to have a negligible influence on the warping properties and stability of planar FREIs. Using these properties, it was shown that the proposed-exact and proposed-approximate equations for estimating the critical load are in excellent agreement for three-dimensional isolators.

The use of the proposed-approximate buckling formulation and the effective warping related properties to predict the stability of FREIs was validated through a finite element parametric study on the stability of rectangular, circular and annular FREIs. The results from the proposed analytical formulation match closely the results from the numerical simulations for all examined bearing geometries. Moreover, it was shown that neglecting warping effects by using Haringx's theory can result in significantly unconservative estimates of P_{cr} for FREIs. Based on these findings, it is recommended that warping effects be considered when evaluating the stability of FREIs by using either the proposed exact or approximate buckling load equation in conjunction with the effective warping properties derived herein. Alternatively, figures providing a reduction factor for the buckling load with respect to Haringx's theory due to warping effects have been provided to facilitate the practical application of these results. Furthermore, in contrast to the case of SREIs, introducing a hole in FREIs was found to severely reduce their stability. Therefore, caution is advised when introducing these modifications in the isolators.

APPENDIX I. EFFECTIVE WARPING PROPERTIES FOR ANNULAR LAYER

The pressure in an annular layer is obtained from solving Eq. (46) with the boundary conditions $p(a, \theta) = p(b, \theta) = 0$. The pressure is given by:

$$p(r,\theta) = \frac{144GS^2}{7\beta^2(1-\eta)^2}\left(\frac{b\phi}{t_e}\right)\left\{\left(\frac{r}{b}\right)^3 + 2\left(\frac{r}{b}\right)\left(\frac{4}{\beta^2}+\omega\right) - 3\eta^2\left(\frac{b}{r}\right) + D_1 I_1\left(\frac{\beta r}{b}\right) + D_2 K_1\left(\frac{\beta r}{b}\right)\right\}\cos(\theta) \tag{63}$$

where $I_m(r)$ and $K_m(r)$ are the modified Bessel functions of the 1st and 2nd kind of order m, and,

$$\begin{aligned} D_1 &= \frac{\left[2\left(\frac{1}{2}+\frac{4}{\beta^2}+\omega\right)-3\eta^2\right]K_1(\beta\eta) - \eta^3\left[1+\frac{2}{\eta^2}\left(\frac{4}{\beta^2}+\omega-\frac{3}{2}\right)\right]K_1(\beta)}{I_1(\beta\eta)K_1(\beta)-I_1(\beta)K_1(\beta\eta)} \\ D_2 &= -\frac{\left[2\left(\frac{1}{2}+\frac{4}{\beta^2}+\omega\right)-3\eta^2\right]I_1(\beta\eta) - \eta^3\left[1+\frac{2}{\eta^2}\left(\frac{4}{\beta^2}+\omega-\frac{3}{2}\right)\right]I_1(\beta)}{I_1(\beta\eta)K_1(\beta)-I_1(\beta)K_1(\beta\eta)} \end{aligned} \tag{64}$$

Enforcing the third and fourth orthogonality conditions in Eq. (3) (and in passing satisfying the first and second conditions), the parameter ω from the warping function is obtained:

$$\omega = \frac{W_1}{W_2} \tag{65}$$

where,

$$\begin{aligned} W_1 &= 12\eta\Big[\beta^2(1+\eta^2)-8\Big] + \beta\Big\{W_3 I_2(\beta\eta)K_1(\beta) + W_4 I_2(\beta)K_1(\beta\eta) \\ &\quad + I_1(\beta\eta)\Big[W_4 K_2(\beta) - W_5 K_1(\beta)\Big] + I_1(\beta)\Big[W_3 K_2(\beta\eta) + W_5 K_1(\beta\eta)\Big]\Big\} \\ W_2 &= 3\beta^2\Big\{8\eta + \beta\Big[\beta I_3(\beta)K_1(\beta\eta) + I_1(\beta\eta)[\beta(\eta^4-1)K_1(\beta) - 4K_2(\beta)] \\ &\quad - \eta^3[4I_2(\beta\eta)K_1(\beta) + \beta\eta I_1(\beta)K_3(\beta\eta)]\Big]\Big\} \end{aligned} \tag{66}$$

and,

$$\begin{aligned} W_3 &= 6\eta^3\Big[8+\beta^2(\eta^2-3)\Big] \\ W_4 &= 6(8+\beta^2-3\beta^2\eta^2) \\ W_5 &= \beta(\eta^2-1)\Big[12(1+\eta^2)+\beta^2(1-8\eta^2+\eta^4)\Big] \end{aligned} \tag{67}$$

Using Eq. (29) for the effective warping rigidity, and Eq. (30) for the areas B and C, these properties are calculated as:

$$\begin{aligned}\widetilde{EJ} = \frac{108\pi GS^2b^4}{49\beta^2(1-\eta)^2}\Bigg\{&\left(\frac{1+2\omega}{\beta}+\frac{8}{\beta^3}\right)\Big[D_1I_2(\beta)-D_2K_2(\beta)\Big]-\frac{2}{\beta^2}\Big[D_1I_1(\beta)+D_2K_1(\beta)\Big]\\&-\left(\frac{\eta^4+2\omega\eta^2}{\beta}+\frac{8\eta^2}{\beta^3}\right)\Big[D_1I_2(\beta\eta)-D_2K_2(\beta\eta)\Big]+\frac{2\eta^3}{\beta^2}\Big[D_1I_1(\beta\eta)+D_2K_1(\beta\eta)\Big]\\&-\frac{3\eta^2}{\beta}\Big\{D_1\Big[I_0(\beta)-I_0(\beta\eta)\Big]-D_2\Big[K_0(\beta)-K_0(\beta\eta)\Big]\Big\}+\frac{1-\eta^8}{8}-9\eta^4\log(\eta)\\&+\left(\frac{4}{\beta^2}+2\omega\right)\left[\frac{1-\eta^6}{3}+3(\eta^4-\eta^2)\right]+(1-\eta^4)\left[\omega\left(\frac{4}{\beta^2}+\omega\right)-\frac{3\eta^2}{2}\right]\Bigg\}\end{aligned} \tag{68}$$

$$B = \frac{3\pi}{7}b^2(1-\eta^2)(1+\eta^2+2\omega) \tag{69}$$

$$C = \frac{9\pi}{98}b^2(1-\eta^2)\Big[3+3\eta^4+8\omega(1+\omega)+2\eta^2(9+4\omega)\Big] \tag{70}$$

The pressure due to an axial displacement Δ, p_Δ, and the effective axial rigidity $\widetilde{EA}$ have been presented by Kelly and Konstantinidis (2011) and are given by:

$$p_\Delta(r) = \frac{48GS^2}{\beta^2(1-\eta)^2}\left(\frac{\Delta}{t_e}\right)\left[1+D_3I_0\left(\frac{\beta r}{b}\right)+D_4K_0\left(\frac{\beta r}{b}\right)\right] \tag{71}$$

$$\widetilde{EA} = \frac{48\pi GS^2b^2}{\beta^2(1-\eta)^2}\left\{1-\eta^2+\frac{2D_3}{\beta}\Big[I_1(\beta)-\eta I_1(\beta\eta)\Big]-\frac{2D_4}{\beta}\Big[K_1(\beta)-\eta K_1(\beta\eta)\Big]\right\} \tag{72}$$

where,

$$D_3 = \frac{K_0(\beta\eta)-K_0(\beta)}{I_0(\beta\eta)K_0(\beta)-I_0(\beta)K_0(\beta\eta)} \qquad D_4 = -\frac{I_0(\beta\eta)-I_0(\beta)}{I_0(\beta\eta)K_0(\beta)-I_0(\beta)K_0(\beta\eta)} \tag{73}$$

Then, the effective warping areas f_B and f_C [Eq. (31)] correspond to:

$$f_B = \frac{12\pi}{7}\frac{\int_{\eta b}^{b}\left[\left(\frac{r}{b}\right)^2+\omega\right]\left[1+D_3I_0\left(\frac{\beta r}{b}\right)+D_4K_0\left(\frac{\beta r}{b}\right)\right]rdr}{\left\{1-\eta^2+\frac{2D_3}{\beta}[I_1(\beta)-\eta I_1(\beta\eta)]-\frac{2D_4}{\beta}[K_1(\beta)-\eta K_1(\beta\eta)]\right\}/(1-\eta^2)} \tag{74}$$

$$f_C = \frac{9\pi}{49}\frac{\int_{\eta b}^{b}\left[9\left(\frac{r}{b}\right)^4+16\omega\left(\frac{r}{b}\right)^2+(8\omega^2+6\eta^2)+9\eta^4\left(\frac{b}{r}\right)^4\right]\left[1+D_3I_0\left(\frac{\beta r}{b}\right)+D_4K_0\left(\frac{\beta r}{b}\right)\right]rdr}{\left\{1-\eta^2+\frac{2D_3}{\beta}[I_1(\beta)-\eta I_1(\beta\eta)]-\frac{2D_4}{\beta}[K_1(\beta)-\eta K_1(\beta\eta)]\right\}/(1-\eta^2)} \tag{75}$$

The solution to the integral in Eq. (74), albeit available, is impractical due to its complexity, while the integral in Eq. (75) does not have a closed-form solution. Nevertheless, both integrals can be solved by numerical integration along the radial direction.

Lastly, the effective bending rigidity for annular bearings is provided for completeness. It corresponds to (Kelly and Konstantinidis 2011):

$$\widetilde{EI} = \frac{48\pi G S^2 b^4}{\beta^2(1-\eta)^2}\left\{\frac{1-\eta^2}{4} + \frac{D_5}{\beta}\Big[I_2(\beta) - \eta^2 I_2(\beta\eta)\Big] - \frac{D_6}{\beta}\Big[K_2(\beta) - \eta^2 K_2(\beta\eta)\Big]\right\} \tag{76}$$

where,

$$D_5 = \frac{K_1(\beta\eta) - \eta K_1(\beta)}{I_1(\beta\eta)K_1(\beta) - I_1(\beta)K_1(\beta\eta)} \qquad D_6 = -\frac{I_1(\beta\eta) - \eta I_1(\beta)}{I_1(\beta\eta)K_1(\beta) - I_1(\beta)K_1(\beta\eta)} \tag{77}$$

This provides all the effective properties required to use Eqs. (6) or (9) for annular FREIs.

APPENDIX II. EXAMPLE CALCULATIONS FOR VERIFICATION

In Table 2, results are presented for each of the effective rigidities and warping-related areas to allow users to verify the proper implementation of the equations; results for the buckling loads are also presented. Three-cases are analyzed: a rectangular bearing with cross-sectional dimensions of 450 mm × 650 mm, a circular bearing with diameter 600 mm, and an annular bearing with outer diameter 600 mm and inner diameter 120 mm. All the cases consist of 33 rubber layers with a thickness $t_e = 6$ mm, interspersed by 32 fiber reinforcement layers with a thickness t_f of 0.5 mm. It is assumed that the rubber has a shear modulus $G = 0.4$ MPa and a bulk modulus $K = 2000$ MPa. The buckling loads presented account for the amplification due to the h/t_r ratio.

DATA AVAILABILITY STATEMENT

All data, models, and code generated that support the findings of this study are available from the corresponding author upon reasonable request.

References

Cowper, G. R. (1966). "The shear coefficient in Timoshenko's beam theory." *Journal of Applied Mechanics*, 33(2), 335–340.

Dikaros, I. C. and Sapountzakis, E. J. (2014). "Generalized warping analysis of composite beams of an arbitrary cross section by BEM. I: Theoretical considerations and numerical implementation." *Journal of Engineering Mechanics*, 140(9), 04014062.

El Fatmi, R. (2007). "Non-uniform warping including the effects of torsion and shear forces. Part I: A general beam theory." *International Journal of Solids and Structures*, 44(18), 5912–5929.

Genoese, A., Genoese, A., Bilotta, A., and Garcea, G. (2013). "A mixed beam model with non-uniform warpings derived from the Saint Venànt rod." *Computers & Structures*, 121, 87–98.

Gent, A. N. (1964). "Elastic stability of rubber compression springs." *Journal of Mechanical Engineering Science*, 6(4), 318–326.

Gent, A. N. and Lindley, P. B. (1959). "The compression of bonded rubber blocks." *Proceedings of the Institution of Mechanical Engineers*, 173(1), 111–122.

Gent, A. N. and Meinecke, E. A. (1970). "Compression, bending, and shear of bonded rubber blocks." *Polymer Engineering & Science*, 10(1), 48–53.

Ghorbi, E. and Toopchi-Nezhad, H. (2023). "Annular fiber-reinforced elastomeric bearings for seismic isolation of lightweight structures." *Soil Dynamics and Earthquake Engineering*, 166, 107764.

Haringx, J. A. (1949). "On highly compressible helical springs and rubber rods, and their application for vibration-free mountings, III." *Report No. Philips Res. Rep. 4*, Philips Research Laboratories, Eindhoven, Netherlands.

Hexagon AB (2021a). *Marc 2021.4 Volume A: Theory and User Information*.

Hexagon AB (2021b). *Marc 2021.4 Volume B: Element Library*.

Kelly, J. M. (1994). "The influence of plate flexibility on the buckling load of elastomeric isolators." *Report No. UCB/EERC-94/03*, Earthquake Engineering Research Center, Berkeley, California.

Kelly, J. M. (1999). "Analysis of fiber-reinforced elastomeric isolators." *Journal of Seismology and Earthquake Engineering*, 2(1), 19–34.

Kelly, J. M. and Konstantinidis, D. (2011). *Mechanics of Rubber Bearings for Seismic and Vibration Isolation*. John Wiley & Sons Ltd.

Lewiński, T. and Czarnecki, S. (2021). “On incorporating warping effects due to transverse shear and torsion into the theories of straight elastic bars.” *Acta Mechanica*, 232, 247–282.

Love, A. E. H. (1944). *A Treatise on the Mathematical Theory of Elasticity*. Dover Publications, New York, 4 edition.

Osgooei, P. M., Van Engelen, N. C., Konstantinidis, D., and Tait, M. J. (2015). “Experimental and finite element study on the lateral response of modified rectangular fiber-reinforced elastomeric isolators (MR-FREIs).” *Engineering Structures*, 85, 293–303.

Papoulia, K.-D. and Kelly, J. M. (1996). “Compression of bonded blocks of soft elastic material: Variational solution.” *Journal of Engineering Mechanics*, 122(2), 163–170.

Pinarbasi, S. and Mengi, Y. (2008). “Elastic layers bonded to flexible reinforcements.” *International Journal of Solids and Structures*, 45(3), 794–820.

Pinarbasi, S. and Mengi, Y. (2017). “Analysis of fiber-reinforced elastomeric isolators under pure "warping".” *Structural Engineering and Mechanics*, 61(1), 31–47.

Simo, J. C. (1982). “A consistent formulation of nonlinear theories of elastic beams and plates.” *Report No. UCB/SESM-82/06*, University of California, Berkeley, Berkeley, California.

Simo, J. C., Taylor, R. L., and Pister, K. S. (1985). “Variational and projection methods for the volume constraint in finite deformation elasto-plasticity.” *Computer Methods in Applied Mechanics and Engineering*, 51(1), 177–208.

Steigmann, D. J. (2017). *Finite Elasticity Theory*. Oxford University Press.

Treloar, L. R. G. (2005). *The Physics of Rubber Elasticity*. Oxford University Press, 3 edition.

Tsai, H.-C. and Kelly, J. M. (2005a). “Buckling load of seismic isolators affected by flexibility of reinforcement.” *International Journal of Solids and Structures*, 42(1), 255–269.

Tsai, H.-C. and Kelly, J. M. (2005b). “Buckling of short beams with warping effect included.” *International Journal of Solids and Structures*, 42(1), 239–253.

Van Engelen, N. C. (2019). “Fiber-reinforced elastomeric isolators: A review.” *Soil Dynamics and Earthquake Engineering*, 125, 105621.

Van Engelen, N. C., Osgooei, P. M., Tait, M. J., and Konstantinidis, D. (2014). “Experimental and finite element study on the compression properties of modified rectangular fiber-reinforced elastomeric isolators (MR-FREIs).” *Engineering Structures*, 74, 52–64.

Van Engelen, N. C., Tait, M. J., and Konstantinidis, D. (2016). “Development of design code oriented formulas for elastomeric bearings including bulk compressibility and reinforcement extensibility.” *Journal of Engineering Mechanics*, 142(6), 04016024.

Table 1. Parameters used for buckling analysis

Parameter	Value
S	10.0, 12.5, 15.0, 17.5, 20.0
S_2^*	2.0, 2.5, 3.0, 3.5, 4.0
ρ[a]	0.5, 1.0, 2.0
η[b]	0.0, 0.1, 0.2

[a] Only applicable for isolators with rectangular cross section
[b] Only applicable for isolators with circular or annular cross section

Table 2. Effective rigidities, warping properties and buckling loads for three example isolators

Parameter	Rectangular isolator	Circular isolator	Annular isolator
b (mm)	225	300	300
ρ	0.69	-	-
η	-	0.00	0.20
A (mm^2)	292,500	282,743	271,434
h (mm)	214	214	214
t_e (mm)	6	6	6
t_r (mm)	198	198	198
t_f (mm)	0.5	0.5	0.5
S	22.2	25	20
β	1.84	2.45	2.45
$\widetilde{EA}$ (kN)	202,951	214,863	128,766
$\widetilde{EI}$ (kN-m^2)	1,381	2,327	2,148
ω	-0.221	-0.256	-0.116
$\widetilde{EJ}$ (kN-m^2)	5.21	8.67	55.29
B (mm^2)	68,023	59,239	61,523
C (mm^2)	56,444	38,378	52,872
f_B (mm^2)	25,090	23,067	42,301
f_C (mm^2)	3,885	18,569	34,949
P_{cr} [Eq. (6)] (kN)	3,553	4,916	2,749
P_{cr} [Eq. (9)] (kN)	3,713	4,876	2,770

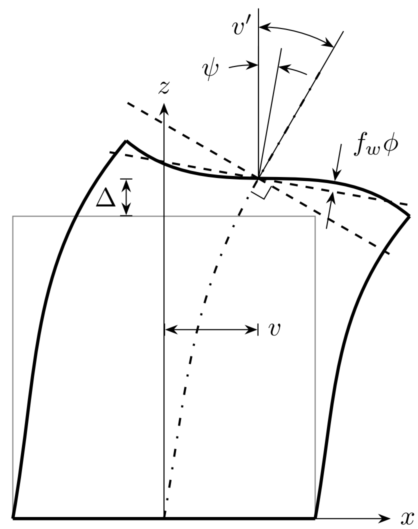

Figure 1. Generalized displacements of the beam

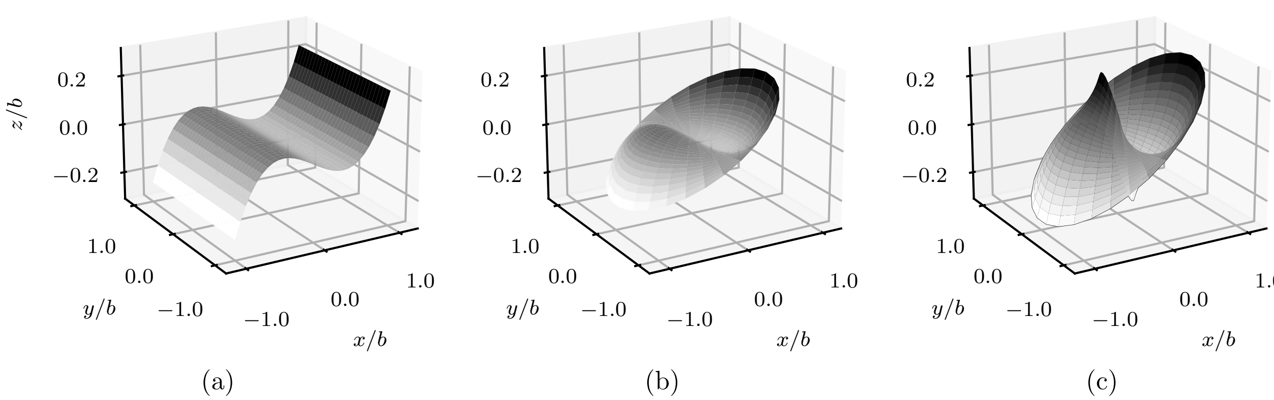

Figure 2. Warping functions for $K/G = 5000$ for (a) square cross section, (b) circular cross section, and (c) annular cross section with $\eta = 0.20$

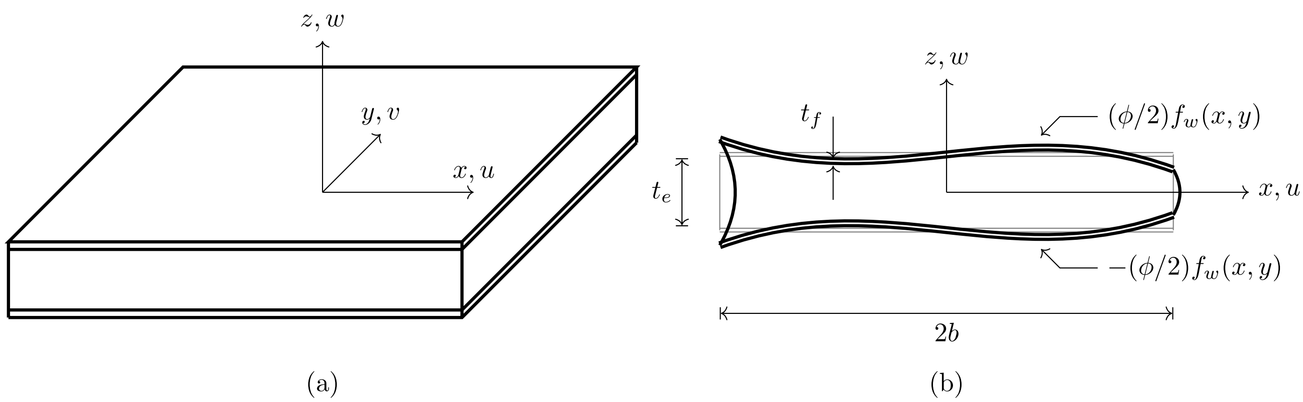

Figure 3. (a) Coordinate system for rubber layer, and (b) warping deformation of rubber layer at $y = 0$

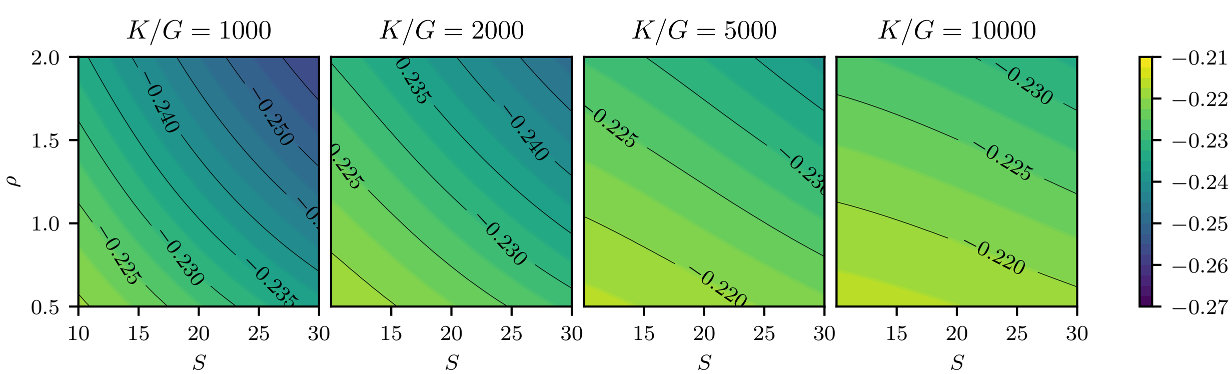

Figure 4. Numerical solution of ω for rectangular cross section

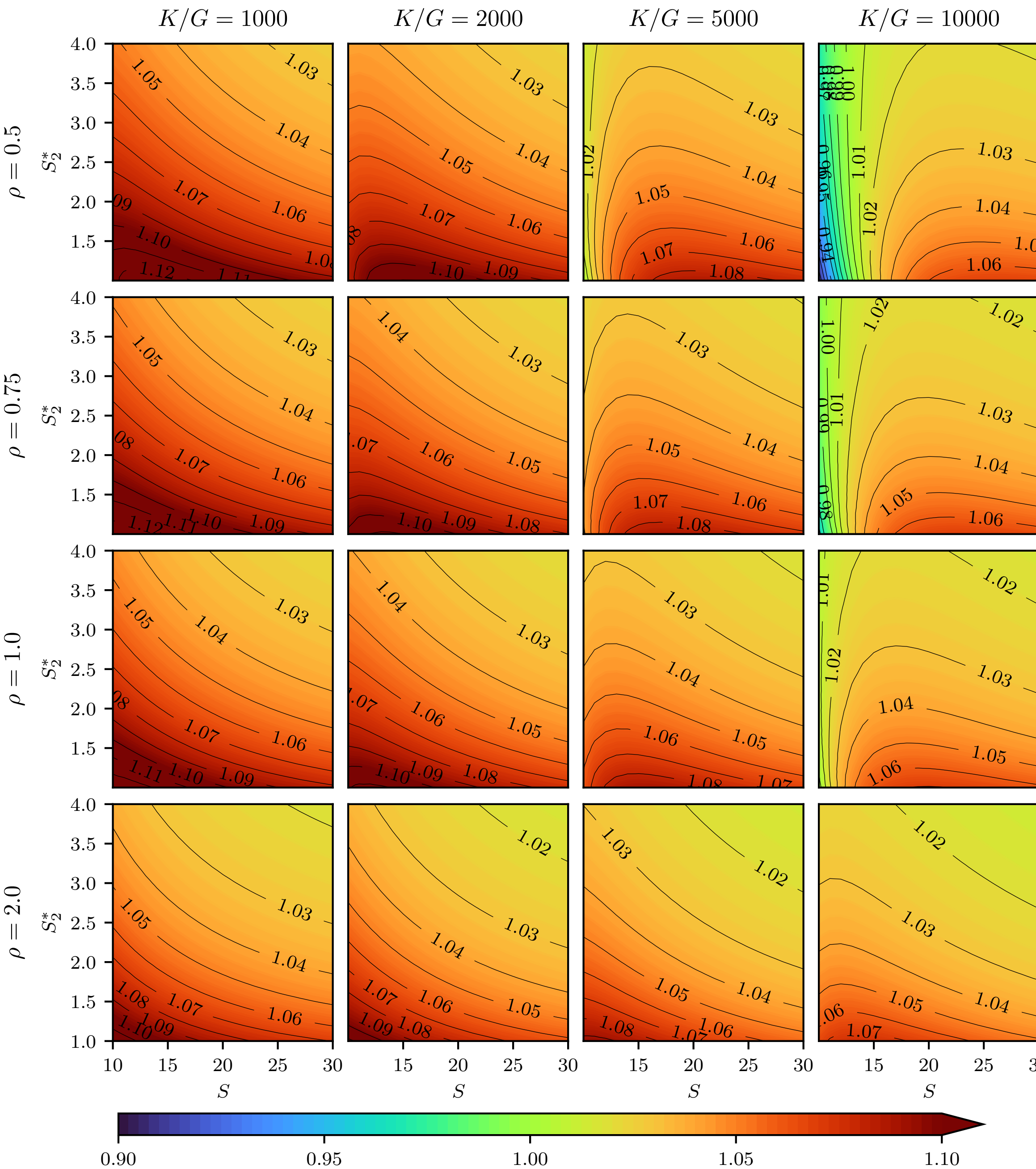

Figure 5. Ratio of P_{cr} from Eq. (9) to P_{cr} from Eq. (6) for rectangular isolators

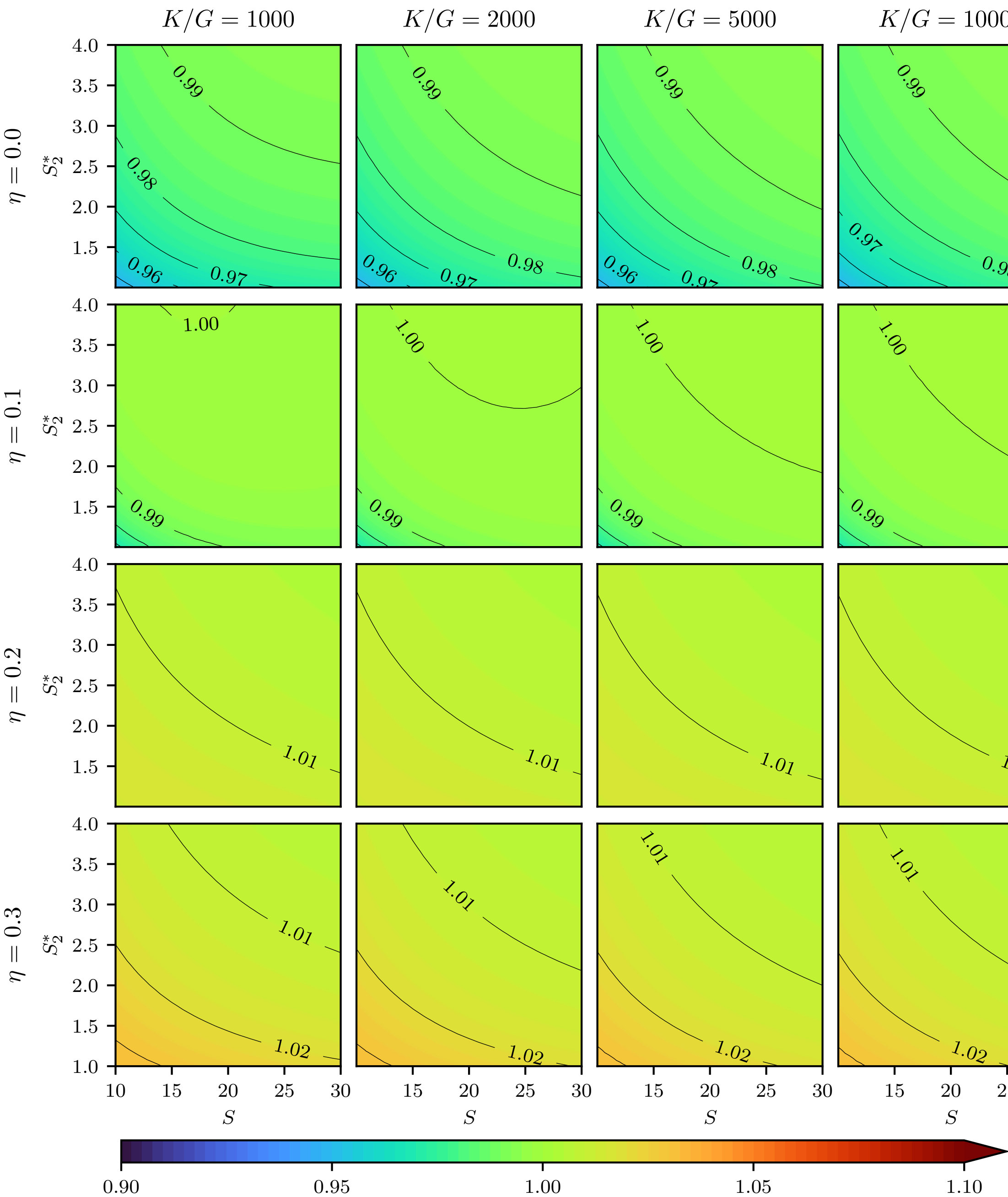

Figure 6. Ratio of P_{cr} from Eq. (9) to P_{cr} from Eq. (6) for circular ($\eta = 0$) and annular ($\eta > 0$) isolators

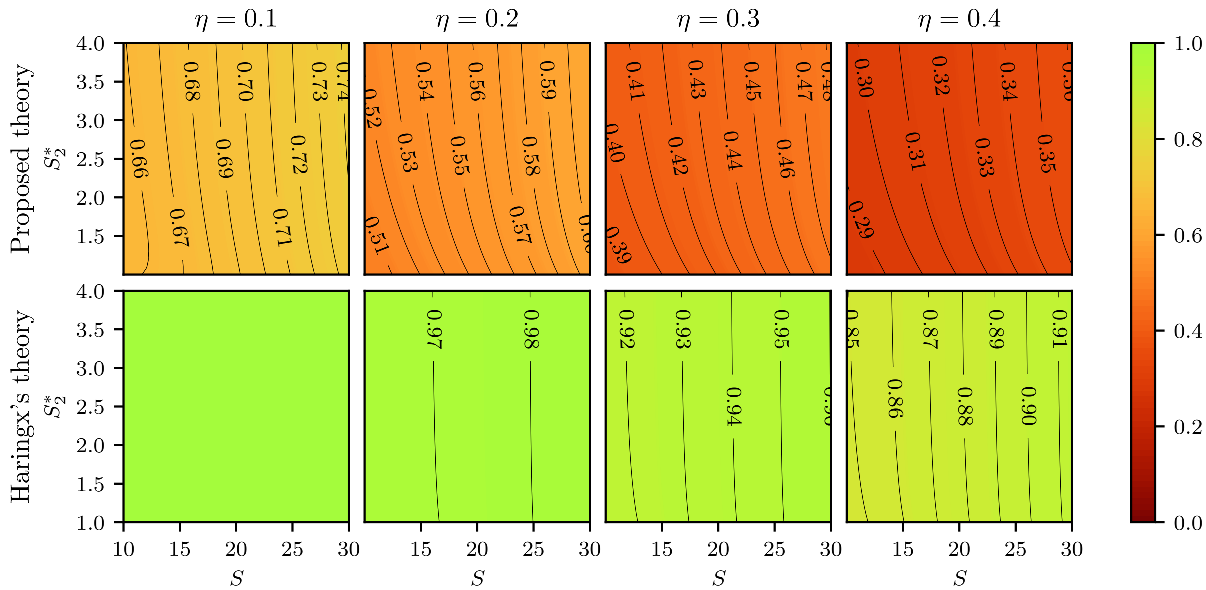

Figure 7. Ratio $p_{cr}^{\text{annular}}/p_{cr}^{\text{circular}}$ for isolators with same b and t_e for $K/G = 5000$

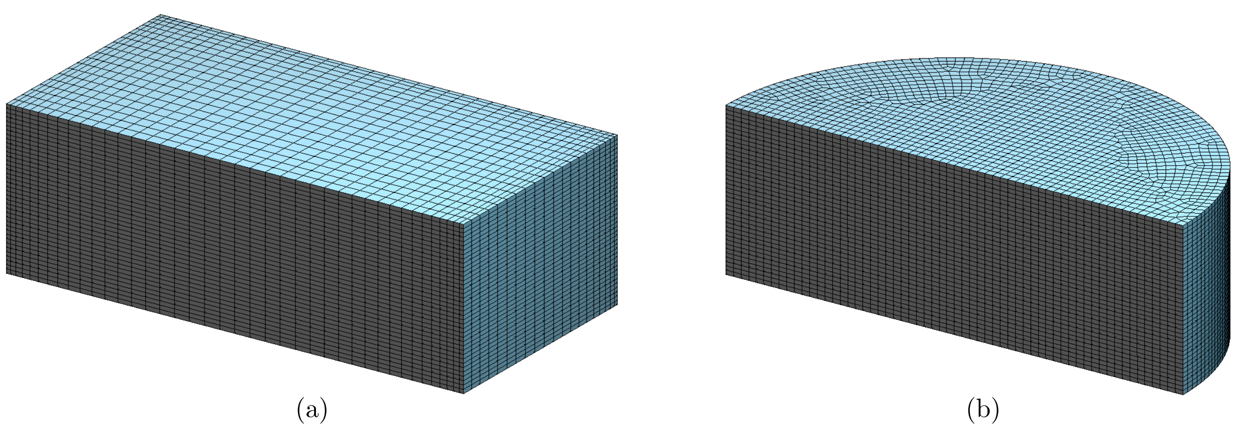

Figure 8. Mesh for (a) square and (b) circular isolator with b = 100 mm, h = 100 mm, and S = 10

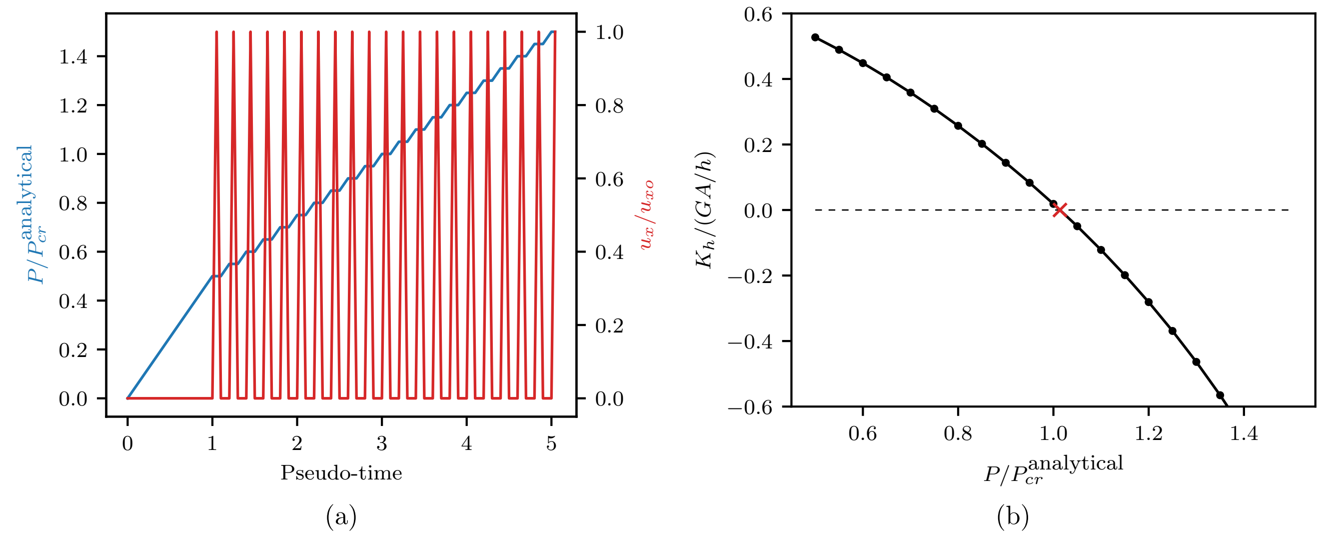

Figure 9. Method applied for estimating the buckling load in the finite element models: (a) loading protocol, and (b) estimation of critical load based on vanishing horizontal stiffness.

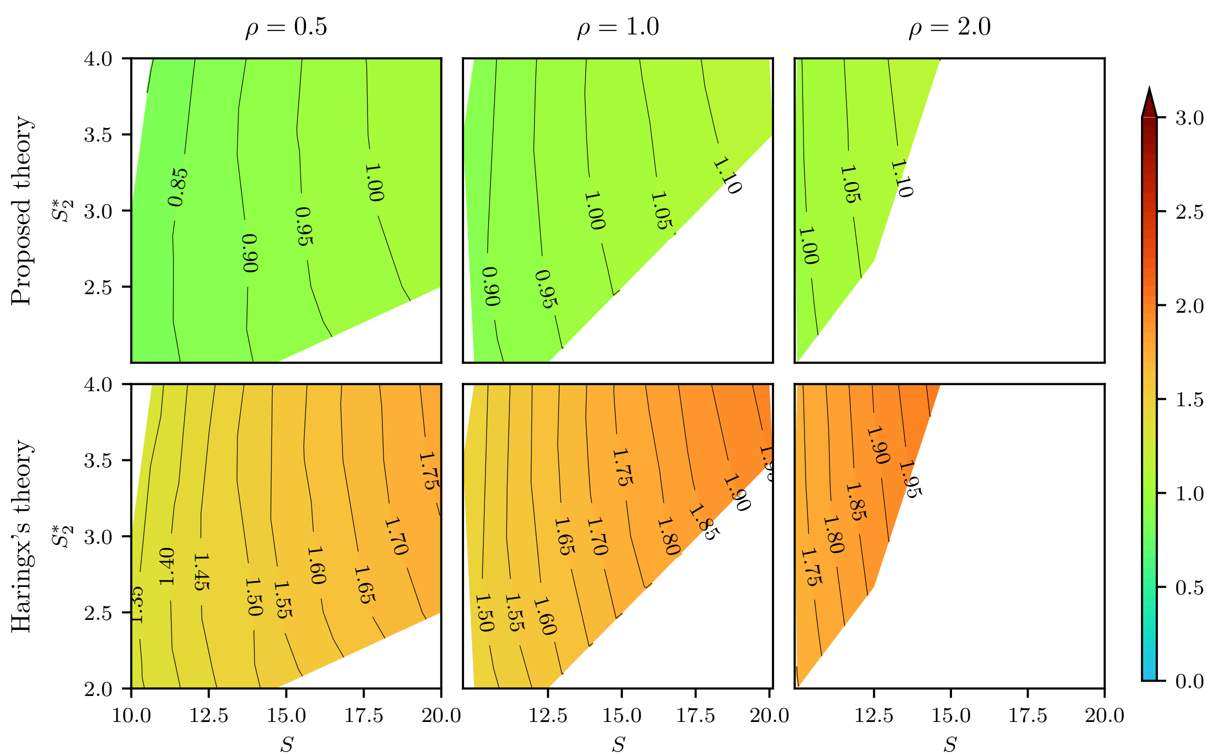

Figure 10. Ratio $P_{cr}^{\text{analytical}}/P_{cr}^{\text{FEA}}$ for rectangular isolators

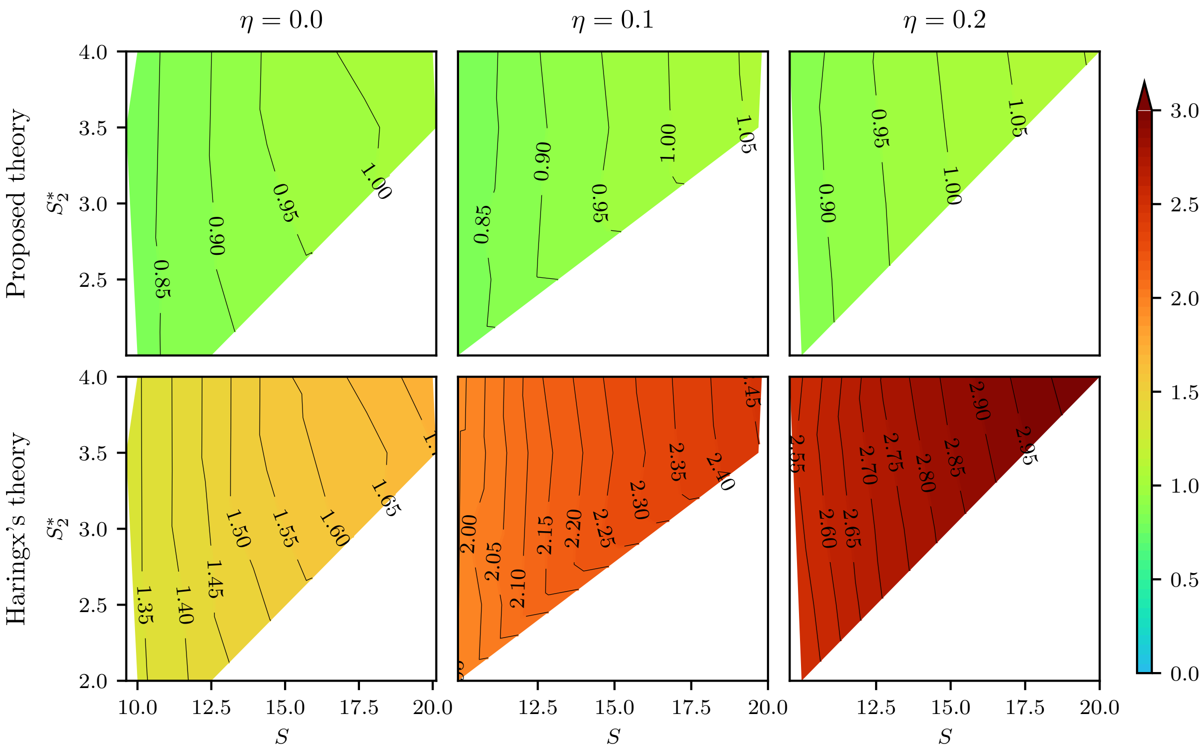

Figure 11. Ratio $P_{cr}^{\text{analytical}}/P_{cr}^{\text{FEA}}$ for circular ($\eta = 0$) and annular ($\eta > 0$) isolators

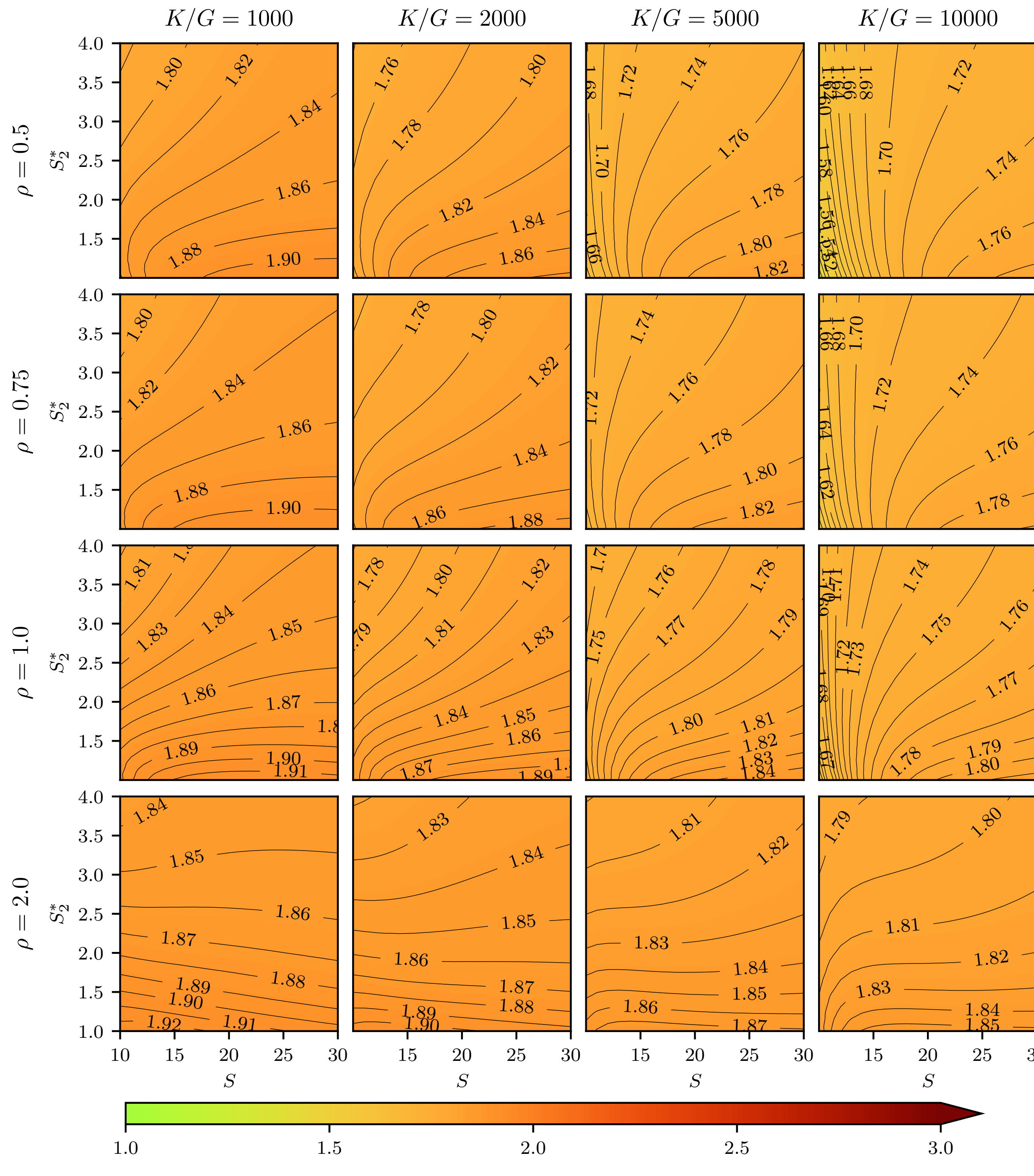

Figure 12. Reduction factor f_R for rectangular isolators

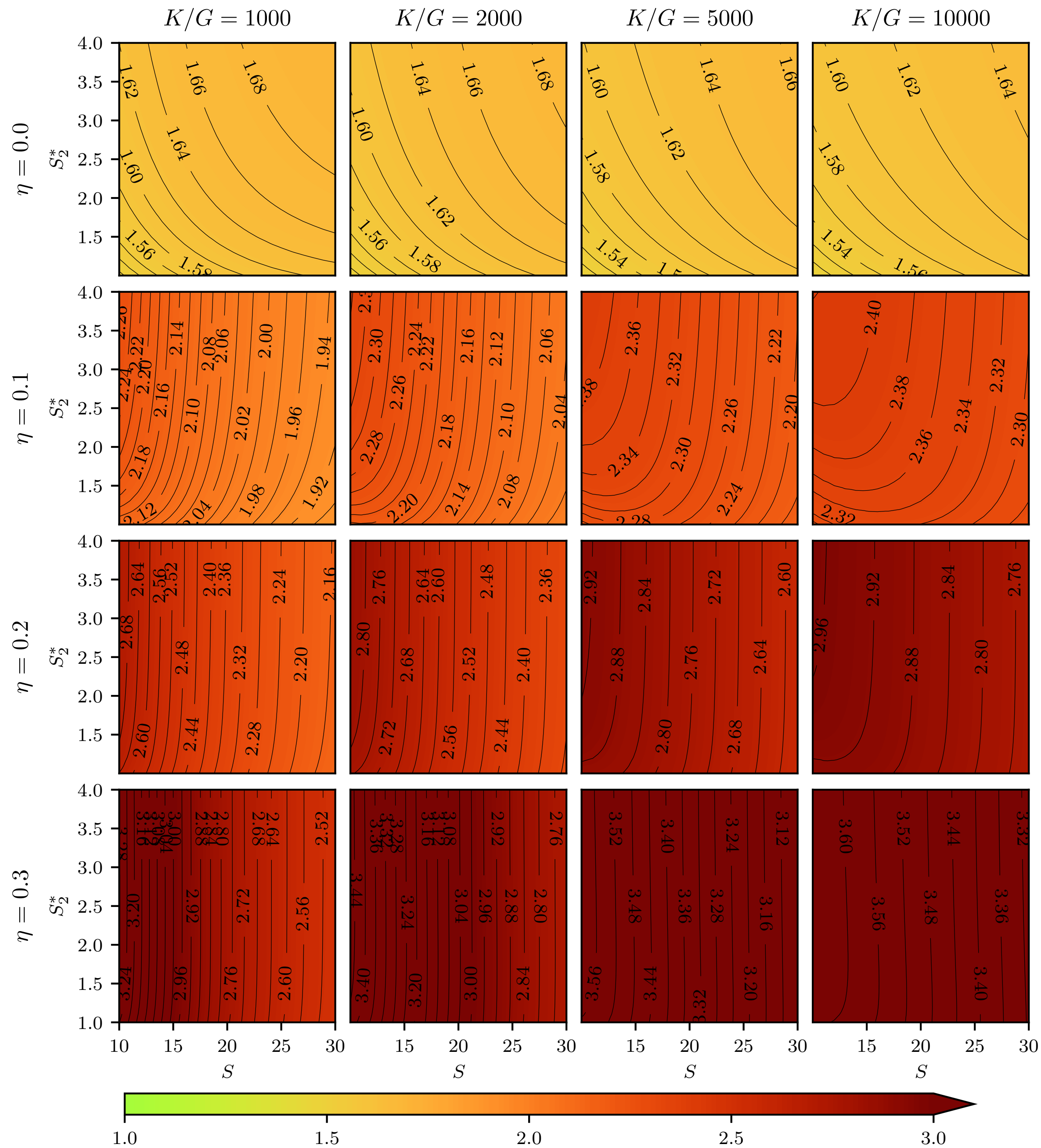

Figure 13. Reduction factor f_R for circular (η = 0) and annular (η > 0) isolators